FEDERAL UNIVERSITY OF SANTA CATARINA
JOINVILLE TECHNOLOGICAL CENTER
AUTOMOTIVE ENGINEERING COURSE

BRUNO CONEHERO DE ASSIS

TRACTION CONTROL SYSTEM APPLIED TO AN ELECTRIC KART

Joinville
2021

BRUNO CONEHERO DE ASSIS

TRACTION CONTROL SYSTEM APPLIED TO AN ELECTRIC KART

Work presented as a requirement for obtaining a bachelor's degree in Automotive Engineering from the Technological Center of Joinville at the Federal University of Santa Catarina.

Advisor: Dr. Andrea Piga Carboni

Co Advisor: Dr. Harald Göllinger

Joinville
2021

BRUNO CONEHERO DE ASSIS

TRACTION CONTROL SYSTEM APPLIED TO AN ELECTRIC KART

This Course Conclusion Work was deemed adequate to obtain a Bachelor's degree in Automotive Engineering, at the Federal University of Santa Catarina, Joinville Technological Center.

Joinville (SC), April 29^{th}, 2021.

Examination Board:

_____

Advisor: Dr. Andrea Piga Carboni
Advisor
President

_____

Prof. Dr. Sérgio Junichi Idehara
Member
Federal University of Santa Catarina

_____

Prof. Dr. Maurício de Campos Porath
Member
Federal University of Santa Catarina

ACKNOWLEDGMENT

This paper was a result from the cooperation between THI and UFSC by means of the German-Brazilian Academic Project Applied Network on Automotive Research and Education (AWARE). The author thanks Bayerisches Hochschulzentrum für Lateinamerika (BAYLAT) for financial support.

I would also like to thank Harald Göllinger, Karin Ebenbeck, Lisa Hermen and Anne-Sophie Kopytynski for helping me to go to Germany and develop this research, as well as providing me support during my stay. Also, the author thanks professor Andrea Piga for the help and support through this thesis.

Lastly, I thank my girlfriend Ana, all my friends and family for assisting me during my graduation, making it easier to face. For all the moments and laughs that I will always remember.

RESUMO

Os sistemas de controle de tração foram desenvolvidos para aumentar a capacidade de tração e, em alguns casos, a estabilidade da direção das rodas motrizes, regulando a taxa de escorregamento dos pneus. Em condições típicas, se o escorregamento do pneu exceder um limite desejado, a relação de escorregamento da roda motriz é regulada para obter o melhor desempenho de direção em uma estrada sob condições de atrito complicadas. Neste trabalho, é apresentado um sistema de aquisição de dados de um Kart elétrico e um controlador de slip limite. A velocidade da roda motriz é ajustada controlando a tensão do motor visando uma relação de deslizamento da roda desejada. Além disso, um modelo Simulink para testar diferentes controladores é desenvolvido e validado. Os resultados dos testes com o Kart validam a ferramenta Simulink e o controlador desenvolvido.

Palavras-chave: Kart elétrico. Sistema de aquisição de dados. Controle de tração. Modelo no Simulink.

ABSTRACT

Traction control systems have been developed to enhance the traction capability and, in some cases, direction stability of the driving wheels by regulating tyre slip ratio. Under typical conditions, if the tyre slip exceeds a desired threshold, the slip ratio of the driving wheel is regulated in order to obtain the best driving performance on a road under complicated friction conditions. In this thesis, an acquisition system to collect data from an electric Kart and a threshold controller is presented. The driving wheel velocity is adjusted by controlling the motor voltage aiming for a desired wheel slip ratio. Also, a Simulink model to test different controllers is developed and validated. Test results with the Kart validate the Simulink tool and the controller developed.

Keywords: Electric Kart. Data acquisition system. Traction control. Simulink model.

LIST OF FIGURES

LIST OF TABLES

LIST OF ABBREVIATIONS AND ACRONYMS

CAN	Controller Area Network
SAE	Society of Automotive Engineers
GC	Gravity Center
ABS	Anti-locking brake system
TCS	Traction control system
VDSC	Vehicle dynamic stability control
ESC	Electronic Stability Control
ECU	Electronic control unit
HCU	Hydraulic control unit
DC	Direct Current
PID	Proportional–integral–derivative controller

LIST OF SYMBOLS

λ	Slip Ratio;
r	Effective wheel radius [m];
ω	Wheel angular velocity [m/s];
μ	Friction Coefficient;
m	Mass of the vehicle [kg];
J_1, J_2	Inertia moment of the front and rear wheels [kgm^2];
F_x	Longitudinal tyre force [N];
F_z	Front wheel load [N];
T_b	Brake torque on each wheel [Nm];
T_w	Driving torque on each wheel [Nm];
L	Distance between the front and rear axles [m];
a	Distance from the front axles to the center of gravity [m];
b	Distance from the rear axles to the center of gravity [m];
h	Height of the center of gravity [m];

TABLE OF CONTENTS

1 INTRODUCTION

After the invention of combustion engines, and the occurrence of the first car accident in 1770, a lot of effort was made to reduce accidents and improve vehicle safety (HART, 2003 apud ALY et al., 2011). This field of research grew with the invention of the first anti-lock braking system (ABS), developed and produced for the aerospace industry (WELLSTEAD; PETTIT, 1997). Not just when braking, but stability is also really important in driving conditions.

Vehicle traction control system (TCS) is one of the vehicle active safety systems that improve the vehicle acceleration performance and stability, especially on slippery roads. It controls the slip ratio of the driving wheel within a reasonable threshold by adjusting the engine torque or brake pressure (KANG et al., 2012). According to Li et al. (2012), the driving torque regulation is used to control the drive wheel slip, and the braking pressure regulation is used to control the difference in the slip rates between two drive wheels.

Although, with really complicated road conditions, there is a need to control both engine throttle and brake pressure, to guarantee vehicle stability and driving performance (KANG et al., 2012). Unfortunately, these two controls penalise each other: excessive brake torque will lower the wheel speed, hence inducing to an increase in the engine output torque. Consequently, a proposal with these two controllers and integrate them to achieve the best control performance is required.

Electronic stability control (ESC) which contemplates active braking system (ABS) and TCS, enables the stability of a car to be maintained during critical maneuvering, operating with brakes and engine management, being really important to vehicle safety and accidents prevention (LIE et al., 2004). According to Aga e Okada (2003), ESC reduced about 35% in single-vehicle accidents with 3 different models of Toyota, and 30% for head-on collisions with other automobiles. Yamamoto e Kimura (1996) studies show that when vehicles equipped with and without ESC were driven around a slippery track, only 5% of drivers with ESC ran out of the lane compared with 45% of drivers whose vehicles were not equipped with ESC.

Even though the results presented previously are promising, track test or driving simulation results may not be replicated in the real world. While reductions in stopping distances were seen on the test track and crash reductions were predicted for vehicles with ABS, studies of real world effectiveness failed to live up to those expectations (FARMER, 2001). In real word cases, there are variables such as driver age, gender, driving experience, seat belt use and others that can't be controlled. Considering this, Lyckegaard, Hels e Bernhoft (2015) concludes that ESC reduces the risk for single-

vehicle injury accidents by 31% when controlling for various confounding factors related to the driver, the car, and the accident surroundings.

With the importance of an ESC explained previously, there are two requirements for this TCS controller algorithm like robustness, since it is really important to the safety of passengers, and acting on different demands of different road conditions, such as each wheel facing a different slip.

This thesis has the aim of building a tool to test different controllers on a kart and also check the viability of constructing this system. After building the measurement system, it is tested and also modelled on Simulink. Also, a different and cheaper solution of velocity sensor is adjusted to check its capability of acquiring the linear velocity. Further, a simple threshold control is applied and validated with the values obtained form the test, to help understand if the Simulink model is able to simulate the kart.

Moreover, this research was concluded in a cooperation from UFSC and THI (Technische Hochschule Ingolstadt) and provided a huge international experience for the author, with access to an electric kart, sensors and equipment that would not be easily available in Brazil. Figure 1 shows the electric kart used in this thesis, recently acquired by the mechatronic laboratory from THI.

Figure 1 – Kart used for this thesis.

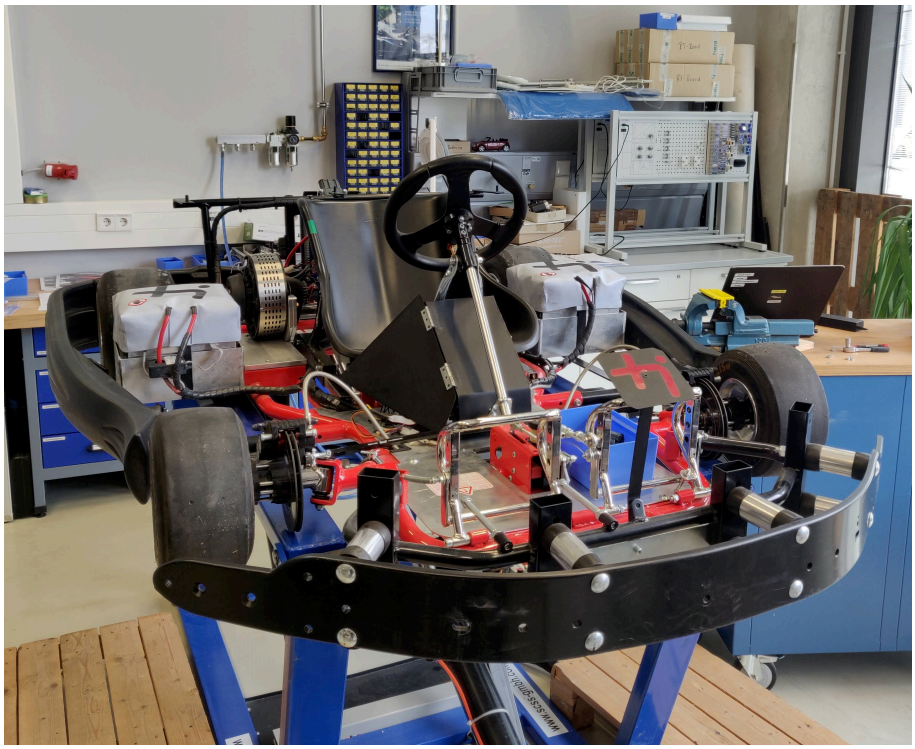

Source: Author (2021).

1.1 OBJECTIVES

In order to establish the correct functioning of the traction control system, the following objectives are proposed in this thesis.

1.1.1 Main Objective

Develop a traction system based on data acquired by a measurement system built on a Kart, testing and validating the results generated by the operation of this traction control.

1.1.2 Specific objectives

- Understand the CAN network and each sensor;
- Integrate the micro controller to act on the Kart traction;
- Create a model of longitudinal movement of the Kart using Simulink;
- Complete an experiment test with the Kart to test the traction control;
- Validate the traction control system created using the data obtained by the Simulink model.

2 LITERATURE REVIEW

This chapter will present a literature review, elucidating the main topics related to the follow-up of this thesis.

2.1 VEHICLE DYNAMICS

Vehicle dynamics is the area that deals with the movement of the vehicle on the track, where the main movements are acceleration, braking and steering. The dynamic behavior of the vehicle is determined by the forces imposed on it by the tyres, gravity and aerodynamics (GILLESPIE, 1992).

The study of vehicle dynamics can be divided into 3 distinct areas, namely longitudinal, vertical and lateral movement. Longitudinal dynamics studies the movement along the X axis and rotations around the Y axis, known as Pitch. The vertical dynamics is represented by the movement on the Z axis and moments generated on the X (Roll) and Y (Pitch) axes on generated by the track. The lateral dynamics is the movement along Y and the moments caused by the actuation on the steering wheel on the Z (Yaw) and X (Roll) axes (GENTA; MORELLO, 2009).

Figure 2 presents the coordinate system proposed by SAE (Society of Automotive Engineers), with the objective of creating a standard in the analysis of vehicle dynamics.

Figure 2 – Coordinate system proposed by SAE.

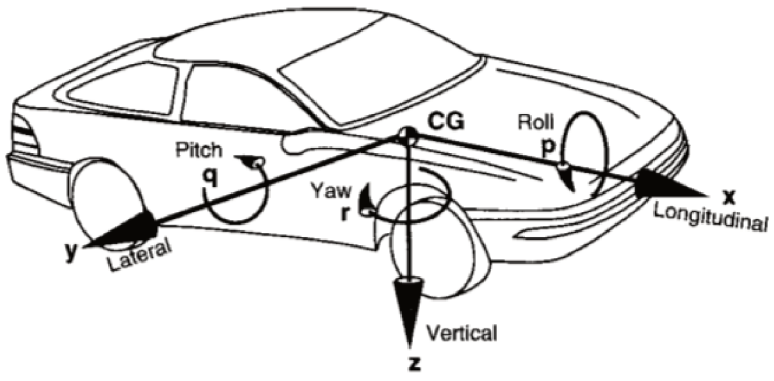

Source: Gillespie (1992, p. 8).

For longitudinal dynamics, according to Gillespie (1992), a single point of mass located in the center of gravity (CG) is sufficient to represent the entire car as a unit, for instance when considering acceleration and braking, without considering weight transfer.

Traction forces are responsible for acceleration and braking as a result of the friction between the track and the tyre (GILLESPIE, 1992). Basically, friction force arise due to the difference between the speed of the track and the tangential speed of the wheels. If this difference is too large, the vehicle loses traction and, consequently, lateral control ability (SAVARESI; TANELLI, 2010).

This difference in speed is known as slip ratio - λ. This value can vary between -1 and 1, depending on which case is experienced. A slip ratio value of 1 corresponds to wheel spin, due to the lack of friction between the track and the tyre. The value of 0 corresponds to pure rolling, and the value of -1 represents locked wheels, in case of a sudden braking, that can cause the loss of control of the vehicle. Equations 1 and 2 are displayed below, for acceleration and braking respectively (WIBEN; ANDERSEN; JENSEN, 2012).

$$\lambda = \frac{V_w - V}{V_w} \tag{1}$$

$$\lambda = \frac{V - V_w}{V} \tag{2}$$

For both equations mentioned above, λ is slip ratio, V is linear velocity of the kart and V_w is the linear velocity of the wheel. The latest can be calculated as described in Equation 3 below, with r being the effective wheel radius and ω the angular velocity of the wheel.

$$V_w = \omega r \tag{3}$$

Since there are two equations that describes the slip ratio, for braking and driving, Figure 3 presents the typical behavior for the longitudinal friction force as a function of slip ratio for each equation.

Figure 3 – Longitudinal friction force as a function of slip ratio.

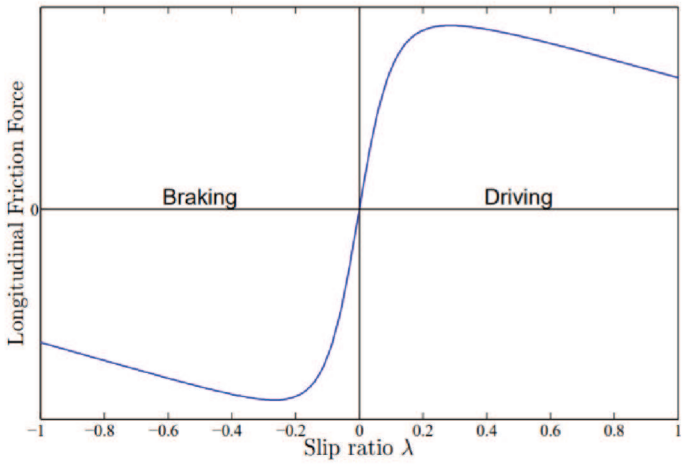

Source: Wiben, Andersen and Jensen (2012)

For this case and in order to improve the behavior of vehicle dynamics, there are systems with the objective of controlling the forces exchanged between tyre and highway (GENTA; MORELLO, 2009). Traction control systems purpose is to maintain an optimal slip ratio as seen in Figure 3, monitoring the speed of the vehicle and wheels, and operating in cases where traction is lost and wheel spins. This optimal slip provides the biggest friction force available for that path, maximizing the torque transmitted from the motor.

For cases of traction control, the vehicle is considered as a rigid body, contemplating only longitudinal and pitch movement. Losses from rolling resistance, aerodynamic resistance and possibly inclination of the track are not considered in this work, nor does their disregard affects the controller (KANG et al., 2012).

A vehicle model is shown in Figure 4 and is considered in the explanation of the following equations.

Figure 4 – Vehicle model.

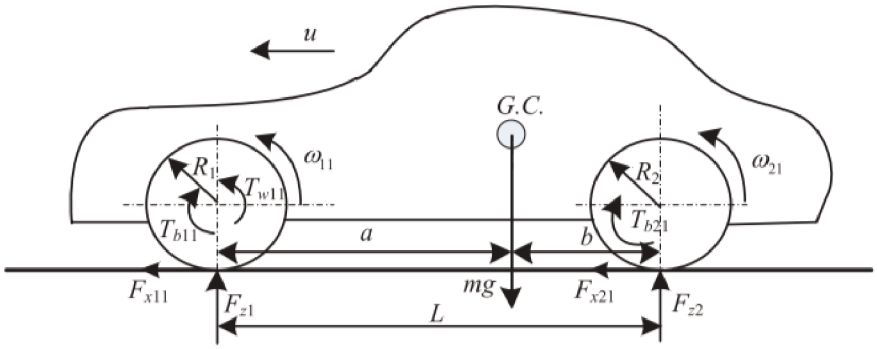

Source: Kang et al. (2012).

Table 1 provides all variables and their description. Subscript i stands for the front ($i = 1$) or rear ($i = 2$) wheels and j evidences left ($j = 1$) or right wheel ($j = 2$).

Table 1 – Figure 4 variables explanation.

Variables	Description
m	Vehicle mass
F_{xij}	Longitudinal tyre force
J	Wheel moment of inertia
ω	Wheel angular speed
R	Wheel effective radius
T_{bij}	Brake torque
T_{wij}	Traction torque
L	Distance from each axle
b	Distance from the rear axle to the center of gravity
a	Distance from the front axle

Source: Author (2021).

The vertical forces on Figure 4 are mg, i.e. the weight force, and F_{z1} and F_{z2} representing the normal force on each wheel. Along with Figure 4 and all terms explained, Equation 4 exemplify the longitudinal motion equation, with u being the longitudinal velocity of the vehicle (KANG et al., 2012).

$$m\dot{u} = F_{x11} + F_{x12} + F_{x21} + F_{x22} \tag{4}$$

Through Figure 4 we can relate the rotation of each wheel of the vehicle with longitudinal force of that tyre and its radius, the torque exerted by the brakes and also the traction torque on the driven wheels.

$$J_1\dot{\omega_{1j}} = -F_{x1j}R_1 - T_{b1j} \tag{5}$$

$$J_2\dot{\omega_{2j}} = T_{w2j} - F_{x2j}R_2 - T_{b2j} \tag{6}$$

Equations 5 and 6 represents the movement of the front and rear wheel, respectively. Traction forces in this case are in the rear wheels because of the Kart presented in this thesis is a rear-wheel drive. As previously explained, i represents front ($i = 1$) or rear ($i = 2$) wheel, while j indicate left ($j = 1$) or right ($j = 2$) wheels (KANG et al., 2012).

2.2 CONTROL SYSTEMS

As explained in the previous section, traction control systems focus on acting and controlling forces exchanged between tyre and track. There are several situations where these traction systems are necessary and their performance is very important for both vehicle stability and passenger safety (ALY et al., 2011).

Most frequent cases where there is a lack of traction happens when accelerating the vehicle on sliding surfaces, during an emergency braking, or even during a curve. This last case can be explained because when the wheel spins or is blocked due to the brake, it supports a limited lateral force, making the curve maneuver difficult (AUSTIN; MORREY, 2000).

In order to get around the problems exposed above, control systems act directly on the wheel speed, as is the case with ABS technology (anti-locking brake system), also applied in TCS (traction control system) and VDSC (vehicle dynamic stability control) (HART, 2003).

For all of these systems, the grip between tyre and track is extremely important and influences slip by changing the torque transmitted to the path and velocity. Slip can be defined using two different functions, one for the case where the wheel locks during braking, and another for when the wheel spins, due to road conditions, as already explained in Equations 1 and 2.

2.2.1 Anti-lock braking system (ABS)

Essentially, ABS is a brake system that prevents wheel locking during an abrupt braking or on sliding surfaces. If the brakes are applied with sufficient force, wheels may lock. Figure 5 shows that for each friction coefficient and wheel slip, there is a region where each velocity is stable and values of slip beyond the critical point at the top of the curve will cause wheel lock (AUSTIN; MORREY, 2000).

Figure 5 – Relation between slip ratio and friction coefficient.

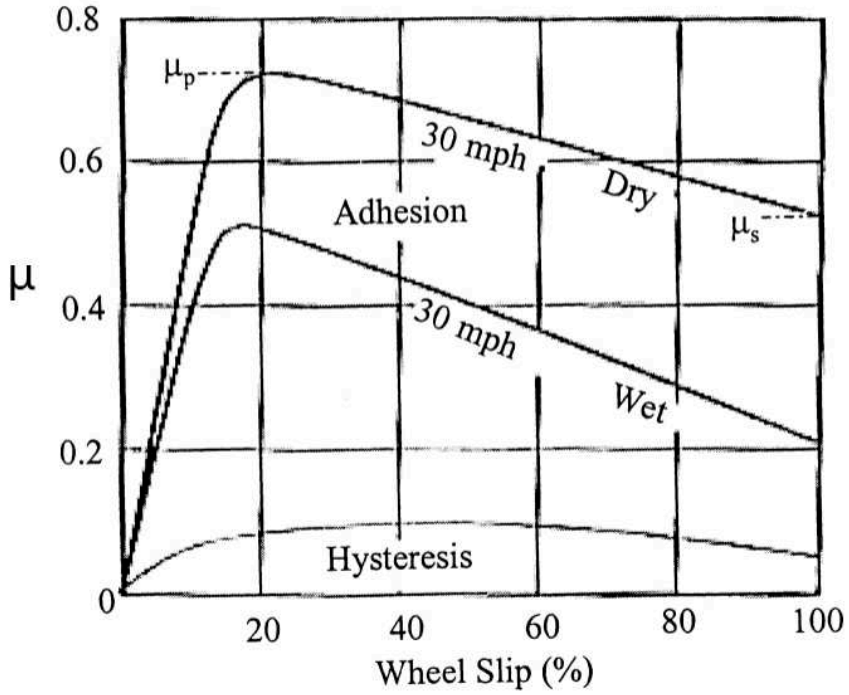

Source: Author (2021).

With the increment in the brake force and consequently slip, the maximum friction coefficient of the stable region decreases, causing the vehicle to enter an unstable region with a lower brake force. From that point on, any increase in brake pressure does not result in an increase in brake force.

The biggest difficulty in the design of an ABS system is the non-linearity and uncertainties regarding the problem. In a simplified way, the project can be reduced to a simple condition logic. The system seeks to keep the slip within the maximum region for the friction coefficient.

Analyzing Figure 5, if slip is greater than 20% for the dry track, the wheels are about to lock or already locked. In that case, the controller must release the brake so that the wheels regain grip.

In the other hand, if the slip has a value less than 20%, the system must maximize the pressure on the brakes so that the braking force increases, thus using all the potential that the relationship between tyre and track guarantees in this situation,

reducing the braking time (WELLSTEAD; PETTIT, 1997).

The logic behind ABS bases only on the speed of the car and speed of the wheel, however the change in the friction coefficient curve for different pavements and difficulty in acquiring the data directly, makes the analysis much more complicated (AUSTIN; MORREY, 2000) than it seems.

2.2.2 Traction control system (TCS)

According to Austin e Morrey (2000), the traction control system represents an extension of the ABS system, since the amount of force that can be transmitted during acceleration is a function that depends on the slip between the tyre and the track.

As the traction control is mainly about regulating the rotation speed of the wheels, it can be accomplished in some ways. Park e Kim (1999) explains how it can be achieved, using one or a combination of methods such as intervention on the accelerator, injection cut out, brake intervention, or limited slip differential control.

Vehicles generally experience problems with traction when passing through two typical cases of road condition. The first case is for tracks with a low μ condition and the other is for tracks with divided μ, that is, one wheel experiences a certain coefficient, while another value of μ influences the other wheel (LIU; JIN, 2016).

The following Figure 6 demonstrates the structure of a standard TCS. The speed information of the wheels and the vehicle reaches the TCS system, which realizes that the wheels are spinning. In this case, the control begins to estimate values of slip ratio and sends the information to the brake and accelerator controller, thereby using these values on the actuator of these two systems, controlling both wheels. The TCS monitors the current speed values to calculate the slip and act on the pressure of the brakes or accelerator at real-time (LIU; JIN, 2016).

Figure 6 – Standard structure of a TCS.

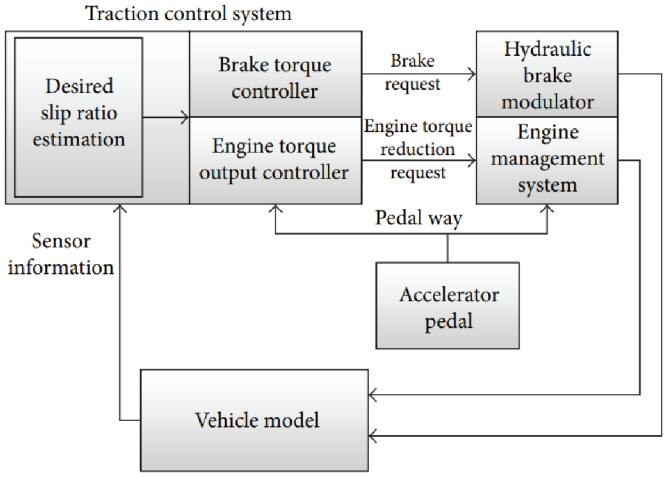

Source: Liu e Jin (2016).

In this work, only the accelerator actuator will be explained and implemented, since the electric motor sends torque for the rear axle and there is only one brake disc for the whole shaft. Therefore, it is not possible to actuate in the brake on one wheel and acceleration for the other wheel as in the case of this thesis it is not independent. The kart has just one brake disc for the entire rear axle, and not independent axles and brakes for each wheel.

Throttle control is possible through an actuator that can move the throttle cable, regardless of the driver's input to the pedal. The injection can be delayed for a few seconds to decrease the engine torque, using the injection map. Likewise it is possible to act on the brakes, restricting the torque on a given wheel. In this case, the wheel signal is sent to the ECU that handles ABS and TCS. The ECU distinguishes between traction or brake slip, and when the wheel spins, it sends the signal to the brake pressure line, regardless of the driver input on the brake as well (AUSTIN; MORREY, 2000).

The controllers act on the methods explained above, both for braking and acceleration cases, and adjust the slip ratio to an optimal value, considering the several different relationships found between tyre and track. For the TCS, it controls just acceleration cases and vary between acting just in the motor, or in brakes, and for some complex controllers for both motor and brakes. Currently, different linear and non-linear control mechanisms are tested in order to evaluate their advantages and disadvantages in traction control systems (LIU; JIN, 2016).

One of the simplest types of control is the threshold method, where a limit value of slip is set, but several experimental tests are necessary to obtain reasonable thresholds for different track conditions (KANG et al., 2012).

Another controller used in these cases is the PID, which does not require a specific mathematical model, but depends on good control parameters. Due to the high non-linearity of the vehicle dynamics systems and large changes in the tyre-road friction, it can generate high control errors (LI et al., 2012). Following this logic, the fuzzy controllers also require several tests to find the appropriate control rules.

Conform the controllers explained above, several tests are necessary so that all cases are included in the control. Looking at Figure 7, we see that for each μ of the track, the longitudinal tyre force curve by slip is different, both in acceleration and in brake.

Figure 7 – Relationship between longitudinal tyre forces and slip ratio.

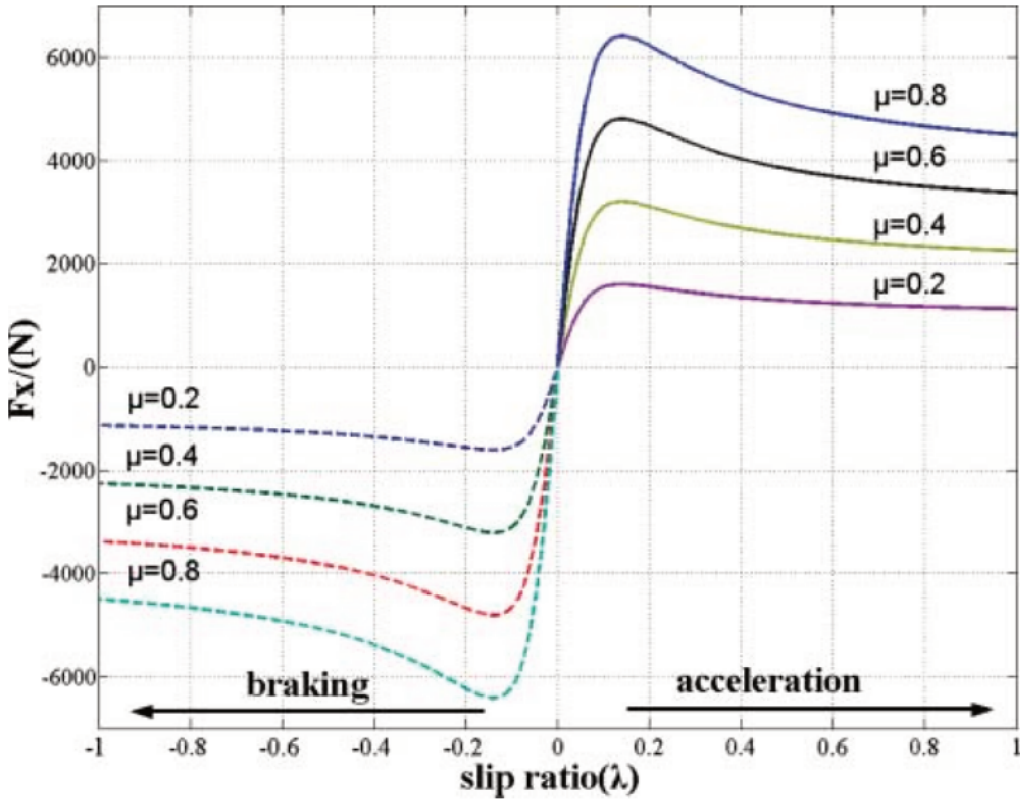

Source: Kang et al. (2012).

After a certain slip threshold, the μ curve enters a state of high non-linearity, making it necessary a more robust controller to deal with that. Analysing Figure 7, the peak of longitudinal tyre force for each μ curve varies, so depending on the μ value, the optimal slip value that results in the maximum force is different. That no-linearity is the biggest obstacle the controller face. Sliding mode control has been widely used and studied for this type of application, as it has a simple and appropriate algorithm for these non-linear situations (KAWABE et al., 1997).

In addition to the formerly quoted methods, Amaral, Göllinger and Fiorentin (2018) proposes the use of neural networks based on reinforcement learning algorithms to improve vehicle handling and stability, by controlling torque during curves.

2.3 CAN NETWORK

The CAN (Controller Area Network) communication network is used to connect different vehicle systems, such as dynamics, propulsion and safety. The ECU of each system transmits and shares its information through the data bus, reducing the possibility of network failure and the number of connections between the systems (BOSCH, 2005).

According to Corrigan (2002), CAN was created by Bosch as a message transmission system with a maximum transmission rate of 1M bit per second. Unlike

traditional networks, such as USB or Ethernet, CAN network does not send large data packets from one node to another, but rather several small messages such as temperature and engine speed for the entire network, ensuring consistency across all nodes in the network.

The main objective of CAN is to connect the control units and sensors, so that the correct action can be taken in the face of a given situation. The data is transmitted in messages containing between 0 and 8 bytes, in addition to the need for a unique identifier so that it is possible to differentiate between simultaneous and active messages originating from different sources, and also designate the priority of the message (ISO, 1993).

For instance, the structure of the CAN bus is formed by two interlaced wires, one wire known as CAN High and the other as CAN Low, both supporting the same amplitude of current, but with opposite directions. Two resistors are added to the edges of the bus bar improving noise immunity and ensuring robustness to interference (CORRIGAN, 2002). Figure 8 presents the structure of a CAN bus, with different nodes attached.

Figure 8 – CAN bus structure.

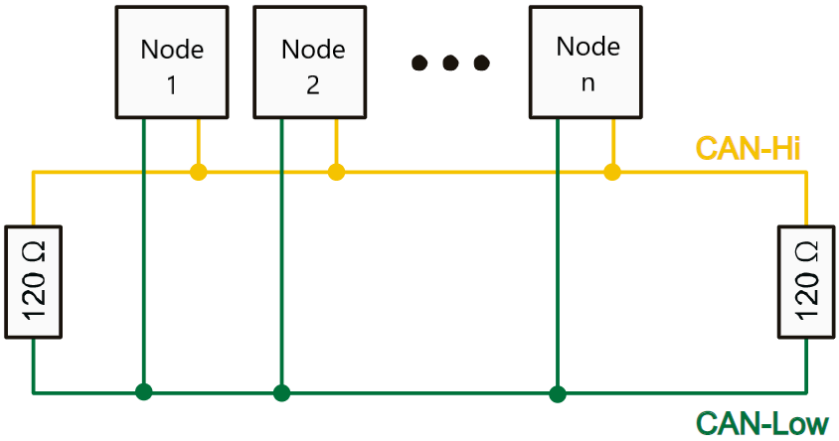

Source: Author (2020).

Furthermore, the use of the identifier to define the priority is the most important part of the CAN network. It is the first part of the message to be transmitted, being from the most significant to the least, with all stations observing the output of the system. If a station transmits a recessive bit (’1’), however it verify that a dominant bit (’0’) is being transmitted by another node, the transmission from the previous station is stopped, since it knows that its message is not the highest priority being transmitted throughout the bus (TINDELL; HANSSMON; WELLINGS, 1994).

If multiple nodes are transmitting messages simultaneously, the message with the lowest binary identifier has priority over the others. Thus all other nodes become receivers during the transmission of the message with the highest priority. At the end

of the transmission, the other nodes may try to relay their messages (BOSCH, 2005; CORRIGAN, 2002).

Figure 9 below shows the structure of a CAN message. There are two types of CAN messages, one with an 11-bit identifier and the other with a 29-bit identifier. Figure 9 displays a message with a 29-bit identifier (CORRIGAN, 2002).

Figure 9 – CAN message structure.

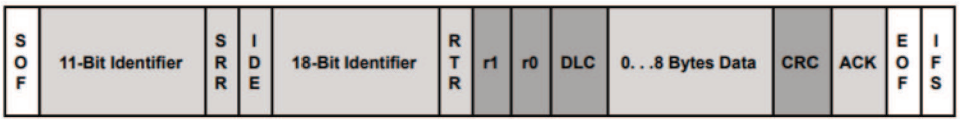

Source: Corrigan (2002).

Being the first field found in the message the SOF (Start Of Frame), indicating the beginning of the message and responsible for synchronizing the nodes of a bus that was inactive. The identifier field contains the message identifier, and as previously explained it is of 29 bits for this example, with 11 bit coming first and then other 18 bit. SRR and RTR represents if the information from this message is important to any other sensor, being dominant if it is. Next field is IDE, and it transmits the information that the identifier is extended and more 18 bit will come. Both r1 and r0 are reserved bits for possible use by future amendment. The DLC (Data length code) section includes the number of data bits contained in the data field. Additionally comes the data field, with the information that the message wants to transmit. The CRC (Cyclic Redundancy Check) field verifies the transmission, whereas the ACK is a confirmation field for the receivers, that all nodes received the message without errors. Finally, EOF (End Of Frame) marks the end of the message (CORRIGAN, 2002).

Figure 10 below shows an example of a CAN message. Some bits were omitted to fit everything in one image.

Figure 10 – Extended CAN message example.

	Start of Frame	Base ID					SRR	IDE	Extended ID					Control						Data								CRC Field					ACK delimiter	End of Frame					
		11 bit identifier							18 bit identifier								Data length code			1 to 8 bytes								15 bits						7 bits					
		ID 10	ID 9	...	ID 1	ID 0			ID 17	ID 16	...	ID 1	ID 0	RTR	Reserved 1	Reserved 0	DL 3	...	DL 0	D 7	D 6	...	D 1	D 0				CRC 14	CRC 13	...	CRC 1	CRC 0		D6	D5	...	D1	D 0
Data	0	0	0	...	1	0	1	1	0	0	...	1	1	0	0	0	0	...	1	0	0	...	0	1				0	1	...	1	0	0	1	1	...	1	1

Source: Author (2021).

3 METHODOLOGY

This chapter sets out the methodology used to develop the design of a data acquisition system in an electric kart, and its subsequent validation in partnership with THI university.

To begin with, the first phase was about project planning. The initial project schedule was built by prof. Harald Göllinger and different topics were considered, taking into account demand from this area of research. This kind of work and test has a lot of difficulties, be it acquiring sensors to measure data or even the car to realize tests. The model developed in this thesis has the aim to settle this demand and provide a tool to test different types of car and control methods.

Initially, the idea was to produce an ABS controller based on a motorcycle ABS, however there was no hydraulic control unit (HCU) available, so in the end the topic chosen was an anti slip control, added to the measurement system. With that in mind, the measurement system started to be applied on the kart, considering which sensors were already available in the laboratory, and already ordering the sensors that were not available. For each sensor that would be installed, its position was evaluated, looking for the best position to avoid noise and interference between sensors, or anything that would disturb the driver.

Table 2 presents a list with all sensors installed in the Kart. Even though not all data from sensors was used in the development of the traction control, these sensors were already installed thinking of future works that could use these variables.

Table 2 – Sensors list.

Sensors	Variable used in TCS?	Range	Unit
Steering Wheel		720°	° (degree)
Acceleration	X	4.2g	m/s^2
Brake Pressure		100 bar	bar
Motor Voltage and Current		150 (V or A)	V and A
Gas Pedal	X	5 Volts	V
Wheel Turn Rate	X	150 Hz	Hz
Velocity	X	100 m/s	m/s

Source: Author (2021).

Before installing all sensors, each one of them was bench tested before being attached to the entire network and checked if it was transmitting any message, and

already analyzed how each message would be treated in order to result in a physical value. As the measurement system moved on, the demand of tests to confirm this system was determined and also the need of a model to validate the test. Figure 11 presents one example of this test for the velocity sensor that was built in this work.

Figure 11 – Test of the velocity sensor.

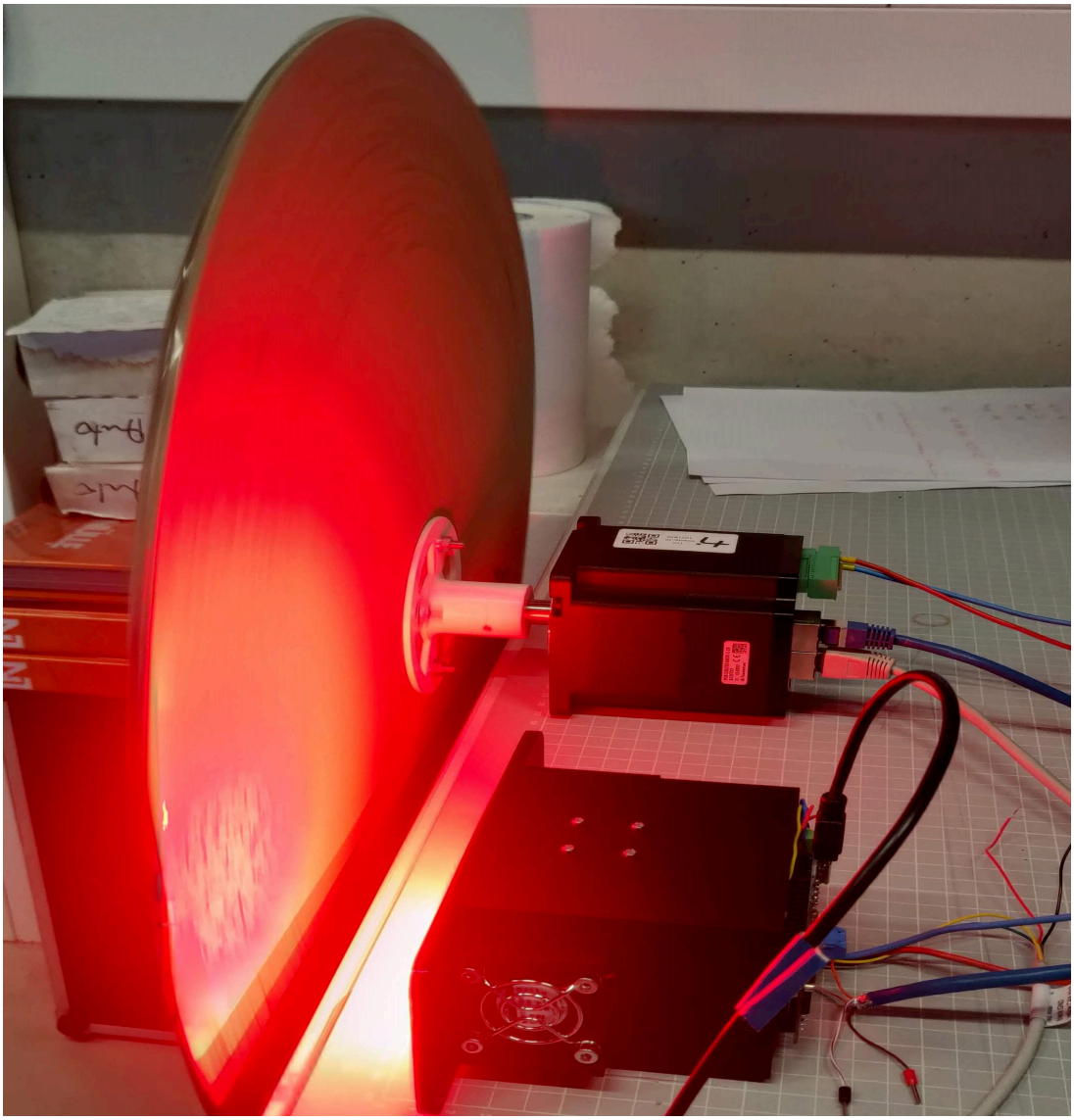

Source: Author (2021).

The sensor is positioned with the same distance that it will be installed in the Kart and a circle cardboard simulates the path moving. Depending on the sensor to be tested, different setups were created. After the measurement system was ready and all sensors were running, the next step was to review literature to model the kart on Simulink aiming to validate future tests. Simulink was chosen because of its simplicity and easy implementation on different micro controllers. The mathematical behind this part is based on Scherf (2011), were different dynamic system are modelled and implemented

on Simulink.

With the model and measurement system running, real tests on the kart were executed to validate the numbers resulted on the model. For the tests, a slippery carpet that was already available on the laboratory was used, adding water with soap to make it even more sliding and the whole setup can be seen in Figure 12.

Figure 12 – Test setup performed on THI.

Source: Author (2021).

The validation is made considering values from the real test and Simulink model created, that will be explained later in this work. Some values are acceptable to be slightly different between both experiments due to a few considerations taken, like the coefficient friction used for the simulation, while this value is not know for the real test. Also, sensors experience small noises and interference, even though some efforts were made to reduce this type of conflict.

4 DEVELOPMENT

In the first place, throughout the next topics I will explain about the Electric Kart, its measures and specifications. These values will be used for this whole section and will assist the development of the Simulink model. Furthermore, it will be described about how the acquisition system was created, all messages generated and choice of sensors. Also, it will be covered about the anti slip controller used for this case.

4.1 ELECTRIC KART

The Electric Kart used for this work was accessible thanks to mechatronic laboratory from THI. Figure 13 presents a general view of the Kart that the controller was applied.

Figure 13 – Electric Kart from THI with motor and electronic highlighted.

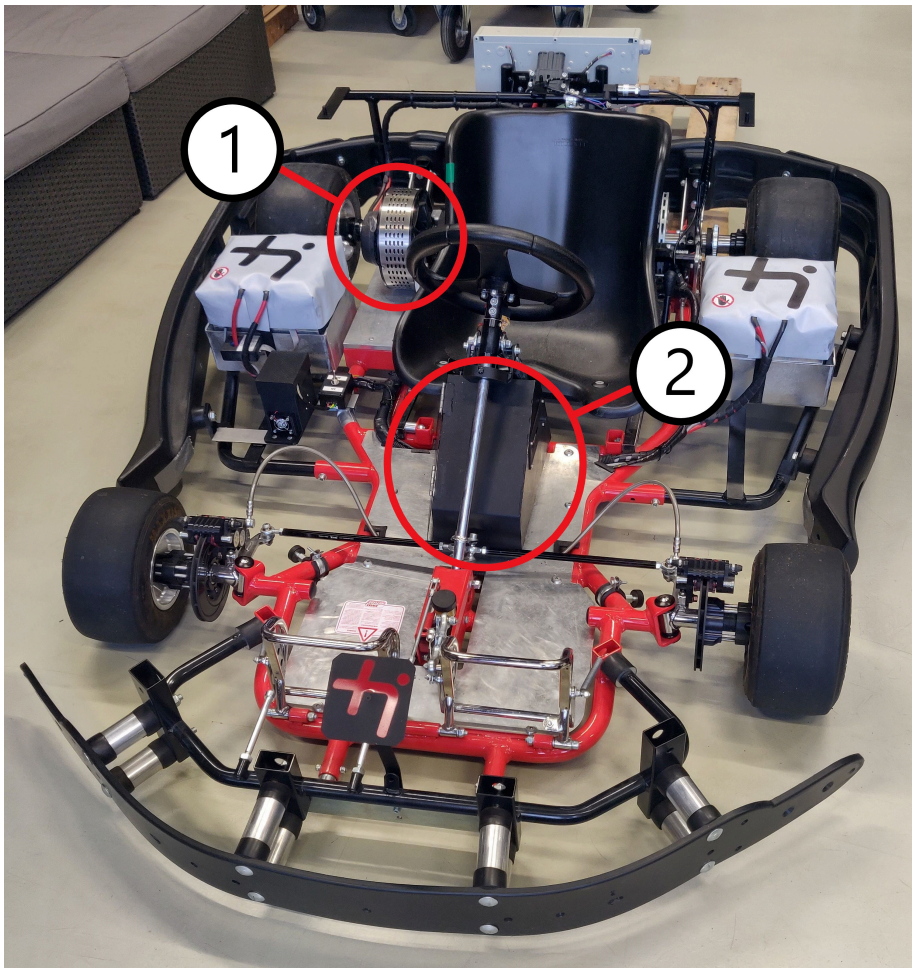

Source: Author (2020).

Initially the Kart was not equipped with any sensor, hence the only electronics

components present at this original state were the parts necessary for the operation of the Kart.

Number 1 is the electric motor from Asmo GmbH. This company uses the same design as Agni and Lynch motors. The model is a Saietta 119 R and it runs with a maximum voltage of 48 V in DC. Table 3 below displays some data from this model. Number 2 presented at Figure 13 represents the components used to handle the electric control of the Kart.

Table 3 – Electric motor data sheet.

Model	rpm/V	max. V	A cont. @48V	cont. output power@48V	max rpm	cont. output power	max. power for 5sec
119-R	58	100	170	7.3 KW	6000	16 kW@90V	ca. 30 kW

Source: Asmo GmbH (2020).

Moreover, the Kart is arranged with two brake discs at the front, and one bigger disc for the rear axle close to the left wheel. Two lithium-ion batteries are installed close to the drivers seat. As well as the dimensions of the Kart and weight are displayed in Table 4. The weight distribution was measured in previous works developed by the mechatronic laboratory from THI.

Table 4 – Kart dimensions.

	Dimensions
Length (mm)	1920
Wheelbase (mm)	1070
Front wheel width (mm)	1200
Rear wheel width (mm)	1270
Weight (kg)	200
Weight distribution $(\%)$	50/50

Source: Author (2020).

4.2 SIMULINK MODEL

With the intention of creating a full model of the kart for future simulations, used to validate different controllers and inputs, the first step was to create a Simulink model. The main goal with that was to emulate every characteristics from the electric Kart, test setup and simplify the tests for different controlling methods.

Instead of setting up a new test for the experimental controller, just add the logic of the controller on the Simulink model and analyze the results, presenting a first

look at the feasibility of this controller for this problem. Finally, the model is displayed in Figure 14.

Figure 14 – Simulink model.

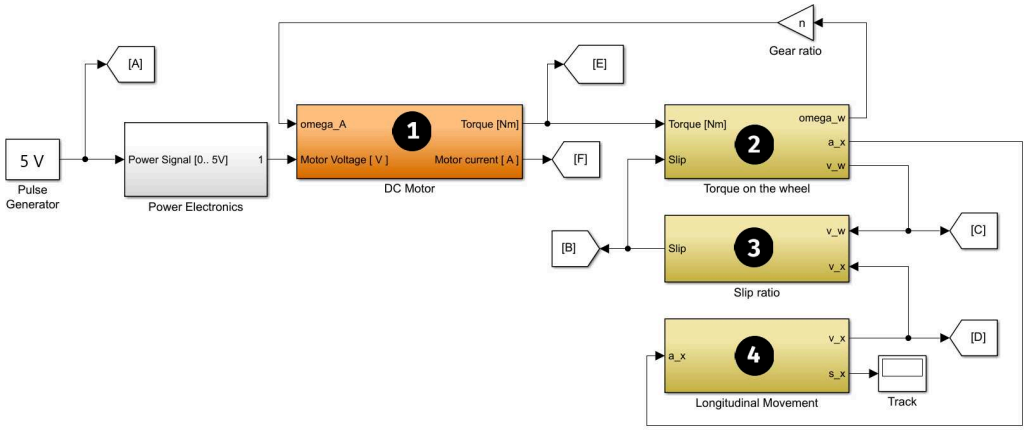

Source: Author (2020).

To begin with, Figure 14 presents an overall overview of the model and all blocks will be covered and explained during this section. With that in mind, the first block explained will be the Pulse Generator, responsible for sending a voltage signal, simulating the motor for the rest of the model. The value for this pulse generated is 5 V, throughout the whole simulation. Even though the picture representing the block on Simulink exemplify an alternate current, the block is configured to send a constant value of 5 V, simulating a DC electric motor.

After that, the pulse generated will enter the Power Electronics block, where it will be multiplied by 48/5, converting the signal to 48 V, as defined earlier as the maximum voltage of the motor. For this reason, Pulse Generator plus Power Electronics emulates the motor at full throttle, sending a signal of 48 V to the rest of model. The control in this case will be on the motor voltage.

Within the Results section of this work, this model was edited with the same controller used on the tests, in that way, values obtained from the model and tests can be comparable and justified.

All over the model there are some blocks with a letter inside, going from A to F. They are responsible to store the value of the variable so all values are tracked during the process. All other blocks contain equations to model the Kart and are marked with a number inside to help over the explanation.

Before describing each block, the model will be analyzed as a whole, tracing inputs until the end. As explained previously, the Pulse Generator emulates the DC electric motor, sending 5 V from the start of the simulation. Next the Power Electronics will multiply that value, increasing it to 48 V as the motor from the kart. Along with this voltage, the angular velocity of the shaft (omega_A) is also needed to calculate torque

and current. Even though omega_A is zero at the start, block 1 will calculate a torque that will feed block 2. This torque will generate angular wheel velocity (omega_w) and taking into account slip, it will also calculate acceleration of the kart (a_x) and wheel linear velocity (v_w).

The wheel angular velocity multiplied by the gear ratio of the axle will return to block 1 as omega_A, working at a closed loop. Kart acceleration (a_x) will enter block 4 and after integrating it, the block will output kart velocity (v_x) and movement (s_x). Kart velocity (v_x) will enter block 3 to calculate slip, together with wheel linear velocity (v_w). This code works with a back propagation, since variables that are calculated at block 4 will propagate backwards and influence the torque calculated at block 1.

Now that the main functionality was explained, each one of the blocks will be clarified with more details. First, before starting with the details from block 1, that handles all equations from the electric motor, it will be presented how the motor was modeled, according to Scherf (2011), and how it was designed inside Simulink. Figure 15 below describes a circuit that represent the electric motor.

Figure 15 – Circuit representing the electric motor.

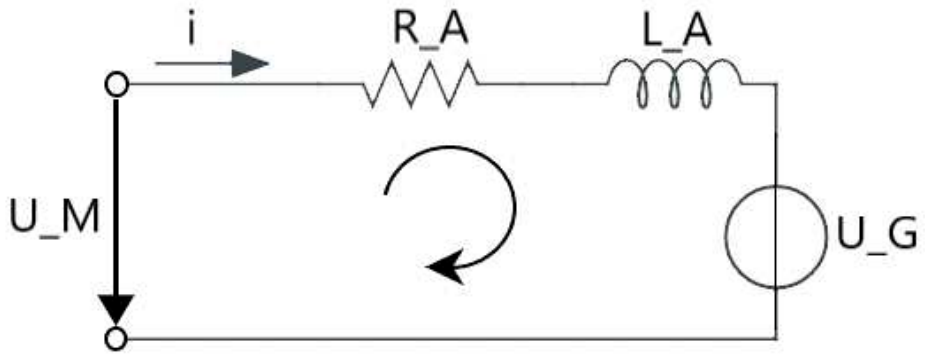

Source: Author (2020).

Accordingly to Figure 15, U_M is the voltage provided to the motor, i the current running through the circuit, R_A is the resistance of the armature, L_A the inductance of the armature and U_G is the voltage that is generated by the electric motor. The fastest the motor spins, the bigger U_G will be, reaching a case where U_G will be greater than U_M, turning the motor in a generator. Resolving the circuit, the Equation that represents is described on Equation 7.

$$U_M = R_A * i + L_A * \frac{di}{dt} + U_G \tag{7}$$

The Equation displayed above represents the mathematical statement for the electric motor, per Scherf (2011). The voltage generated by the electric motor, U_G can also be expressed as the torque constant of the motor multiplied by the angular velocity of the shaft, like Equation 8 declare beneath.

$$U_G = k_g * \omega_A \tag{8}$$

Considering Equation 8 into Equation 7 and isolating the derivative term of the Equation 7, the electric motor can be modeled by Equation 9 shown below.

$$(U_M - R_A * i - k_g * \omega_A) * \frac{1}{L_A} = \frac{di}{dt} \tag{9}$$

Alongside Equation 9, the last task is to implement the mathematical model on Simulink. Figure 16 reveals how the blocks are arranged inside block 1, in order to calculate motor current (A) and torque of the motor (Nm), and will be explained below.

Figure 16 – Block 1 view (DC motor equation).

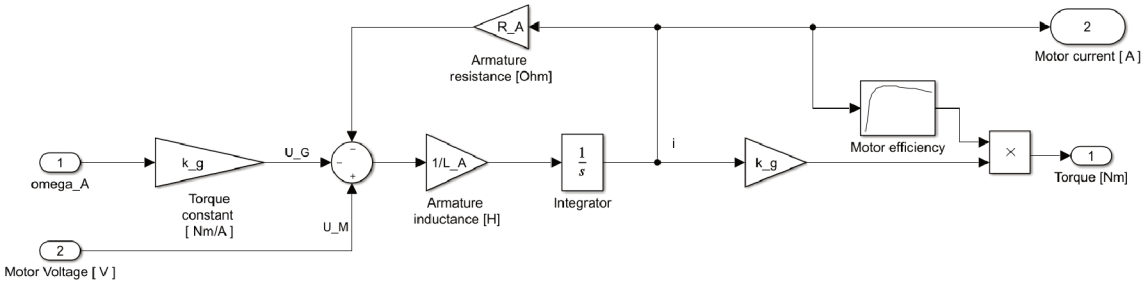

Source: Author (2020).

Entering the sum round block on the left side there is the $K\_g * omega\_A$ and U_M, similarly, coming at the top is the $R\_A * i$ part of the Equation. With the sum of these elements they are all multiplied by $1/L\_A$ and followed by an integration over time, producing i, the current of the motor. Two different variables are produced as output of this first block, those being the motor current and torque, with the latest produced by multiplying the current with the torque constant and motor efficiency.

Table 5 show the values and names for the variables that are exhibited in Figure 16 and will be part of the next blocks also. Furthermore, all variables used in the model are loaded into Simulink from a Matlab file that is fully displayed in Appendix A.

Table 5 – Variables loaded from Matlab file.

	Value	Variable
Effective radius $[m]$	0.135	r
Torque constant $[Nm/A]$	0.15	k_g
Armature resistance $[Ohm]$	0.0225	R_A
Armature inductance $[H]$	23e-6	L_A
Kart mass $[kg]$	200	m

Source: Author (2020).

Particularly in Figure 16, there is a block named Motor Efficiency, with values for efficiency that range from 30% to 83.7%.

Following the steps from Figure 14, the torque that was calculated in Block 1, is used as an input along with the slip for Block 2. Therefore, Block 2 takes the torque and slip, as well as a μ-slip curve to interpolate and obtain μ values for each slip. Not only the slip, it also measures acceleration (a_x), wheel linear velocity (v_w) and wheel angular velocity ($omega\_w$). Figure 17 illustrate the view from inside Block 2.

Figure 17 – Block 2 view (Torque on wheel).

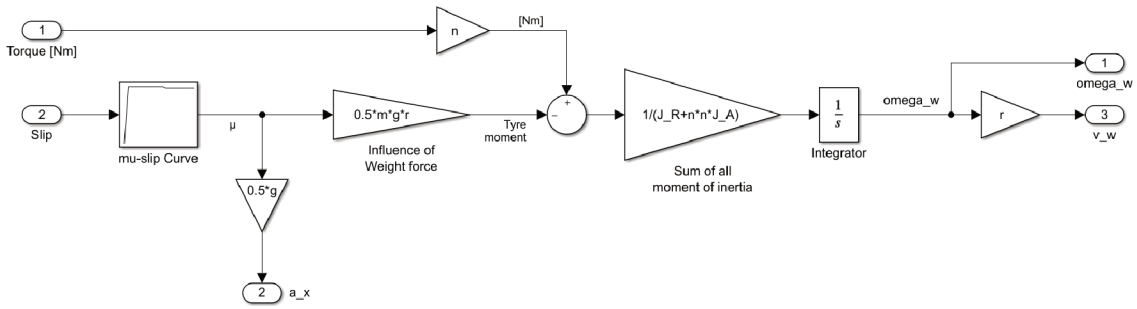

Source: Author (2020).

At the beginning of Block 2, for each slip received a μ can be interpolated. The torque from the motor will be multiplied by n that is the number of teeth, so the result will be the torque on the wheel. With the coefficient of friction and both inputs, the acceleration and velocities are achievable. Firstly, acceleration of the Kart is calculated after manipulating Equation 10.

$$\mu N = m * a\_x \tag{10}$$

Where N is the normal force and calculated as in Equation 11, considering that the weight is distributed evenly throughout the kart.

$$N = \frac{mg}{2} \tag{11}$$

In this thesis, weight transfer is not considered, so the normal force on the rear axle is considered to be half of the total weight. Hence, with the combination of Equations 10 and 11, the Equation 12 presented below represents how a_x is calculated as shown in Figure 17.

$$a\_x = 0.5\mu g \tag{12}$$

Consequently, Equation 13 calculates all torque that is lost due to friction between tyre and road also described in this thesis as Tyre moment just as in Figure 17.

$$Tyre\ moment = N * \mu * r \tag{13}$$

Therefore, torque from motor is reduced by this tyre moment calculated. This resulting torque is multiplied by the sum of all moment of inertia, both from wheel (J_R) and motor (J_A), producing angular acceleration for wheels. After integrating the angular acceleration over time it becomes angular velocity ($omega\_w$) and multiplying it by r, the result is wheel linear velocity (v_w).

After all, Block 4 takes as input the acceleration calculated at the previous block, and integrates two times over time, one to produce linear velocity of the Kart, and for the second time to achieve distance traveled, just as exposed in Figure 18.

Figure 18 – Block 4 view (kart velocity and movement).

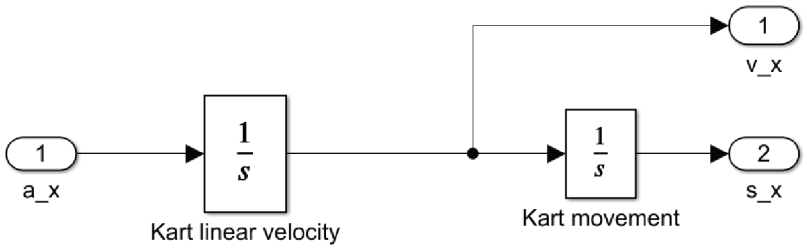

Source: Author (2020).

Finally, this velocity from Block 4 is used along with the wheel linear velocity generated from Block 2 to calculate slip on Block 3. Equations 1 and 2 used for this calculus, depending upon the case, were already presented on Section 2.2. Figure 19 displayed beneath contains both functions inside the middle block, in order to calculate slip using v_w and v_x.

Figure 19 – Block 3 view (slip calculus).

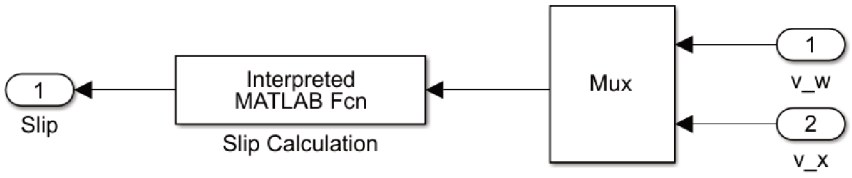

Source: Author (2020).

The slip function used here is the same as Equation 1 that was explained before.

4.3 DATA ACQUISITION SYSTEM

During this section, everything about the data acquisition system will be covered, going from the model of each sensor, how each CAN message is structured and how to obtain the physical value for that sensor from the message. In addition, all sensors that were installed and later will be explained are listed below. Figure 20 shows a complete view of the kart and where all sensors were installed.

Figure 20 – Kart with all sensors positions.

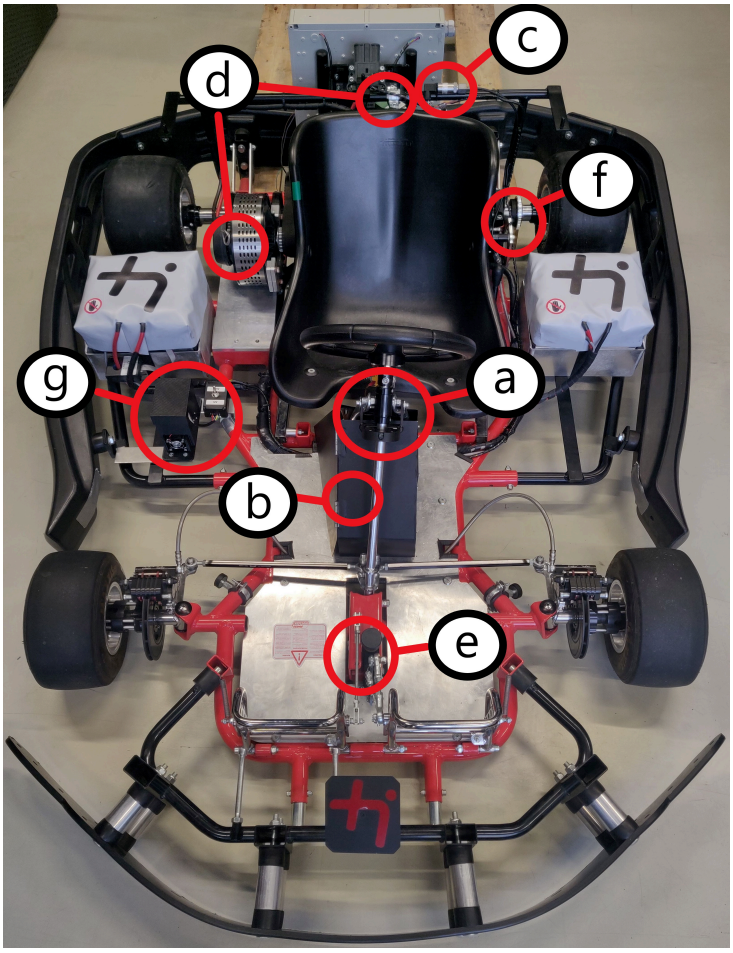

Source: Author (2020).

a) Steering Wheel (degrees)
b) Acceleration from Bosch
c) Brake Pressure (bar)
d) Motor Voltage and Current (V/A)
e) Gas Pedal (potentiometer)
f) Wheel Turn Rate (Hall sensor)
g) Kart linear velocity

Accordingly to section 2.3 and how CAN messages are structured, Table 6 displays the structure for all messages from the sensors used on this thesis. Depending

on the number of sensors attached on the same ID, the number of bytes can vary. Each data from one sensor represents two bytes, so it can cover all range of values for that variable. The message is defined by hexadecimal values and of type Intel, so in order to obtain its value it is required to switch bytes.

Table 6 – Message from Analog 2 box.

ID	Byte (Intel)							
250	0	1	2	3	4	5	6	7
Hex values	03	00	17	01	12	00	1A	00
	motor current		brake pressure		motor voltage		gas pedal	

Source: Author (2020).

If brake pressure, for example, is represented by bytes 2 and 3, the number that express that value would be 17 01 (Intel), in a hexadecimal format. As it is in the Intel format, the real value is 01 17 and converting it to decimal and binary formats is 279 and 100010111, respectively. All sensors have a factor to multiply and offset to subtract or add to the raw value from the message and obtain the physical value as show in Equation 14.

$$\text{physical value} = \text{CAN data} * \text{factor} + \text{offset} \tag{14}$$

Concluding, it is possible to convert a hexadecimal number to a digit format and manipulate it to obtain a physical value that can represent the value of the variable from each sensor. Each sensor has its own factor and offset, be it from the data sheet of the sensor or acquired with bench testing. And as every two bytes from Table 6 represents data, it is possible to get a physical value for all sensors, just using different values for Equation 14.

4.3.1 PCAN MicroMod box

For some sensors, the output signal is not an already built CAN message because these sensors don't have a CAN module integrated, so their output signal is a voltage signal. In order to read and transmit this signal to other sensors, a PCAN MicroMod box from PEAK System was used to receive the voltage signal from the sensor and transmit a CAN message, as shown in Figure 21.

Figure 21 – PCAN MicroMod box.

Source: Author (2020).

Using the PCAN MicroMod configuration software, it is possible to setup the ID, length of the message and how the digits will vary according to the voltage. The sensors that were installed to the PCAN boxes were:

- Brake Pressure
- Motor Voltage and Current
- Gas Pedal
- Wheel Turn Rate

Brake pressure, gas pedal and motor voltage/current were all installed at the PCAN MicroMod Analog 2 (right), and wheel turn rate was installed at PCAN MicroMod Mix 2 (left), as Figure 22 shows.

Figure 22 – PCAN boxes installation layout.

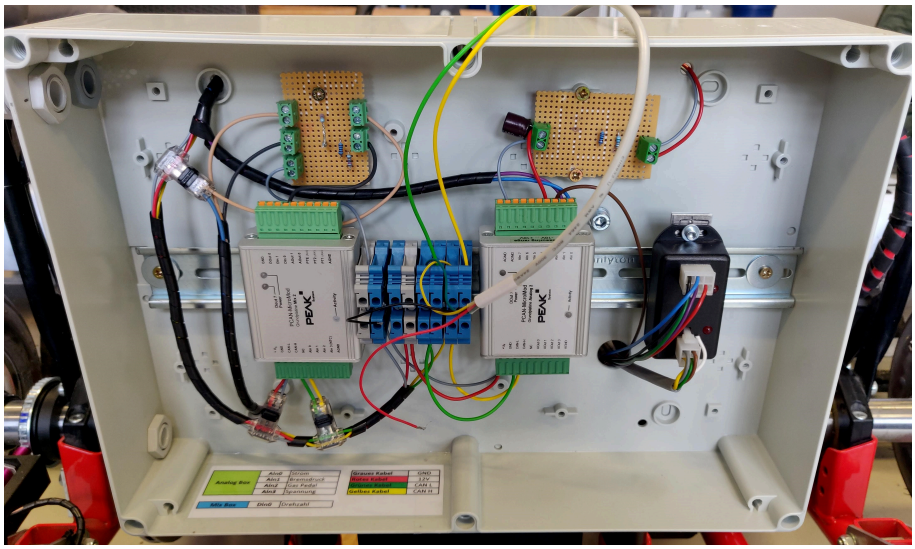

Source: Author (2020).

The reason why wheel turn rate was installed in another box is that the Mix 2 has one frequency input port, the type of output for the turn rate sensor, while the Analog 2 only has analog inputs. Both boxes are connected to the battery of the kart and the CAN network, the first group of cables going left to right. Above the boxes there are two circuit boards that work as voltage dividers, to protect the PCAN boxes. The one connecting to Mix 2 is the voltage divider for the turn rate sensor, and the one at the right is for the motor. Between both boxes there are some connectors, to make the layout cleaner, and at the right there is a black box that is part of the installation of the MillipaK controller, from Sevcon company, and it is responsible for powering the kart and its operation.

After installing and configuring both PCAN MicroMod boxes, the messages generated from both devices are described as in Tables 7 and 8.

Table 7 – Message from Analog 2 box.

ID	Byte (Intel)			
	0 1	2 3	4 5	6 7
250	motor current	brake pressure	motor voltage	gas pedal

Source: Author (2020).

Table 8 – Message from Mix 2 box.

ID	Byte (Intel)			
	0 1	2 3	4 5	6 7
240	turn rate	–	–	–

Source: Author (2020).

For the steering wheel sensor and the kart velocity, both sensors have their own CAN module, so they were installed directly to the CAN bus network.

4.3.2 Steering Wheel Sensor

First, the steering wheel sensor used was from Bosch, model number 0 265 005 411. This sensor model is really common when talking about steering data and can be easily found.

As predicted, this sensor needs to be placed around the steering bar of the kart, so it can measure the angle. To hold it in a fixed position, it was created a housing using CATIA software and printed it using a 3D printer. A support was also created as the bar has a smaller radius comparing to the sensor. Figure 23 shows the steering wheel sensor and the support already installed over the bar.

Figure 23 – Steering wheel sensor with the support.

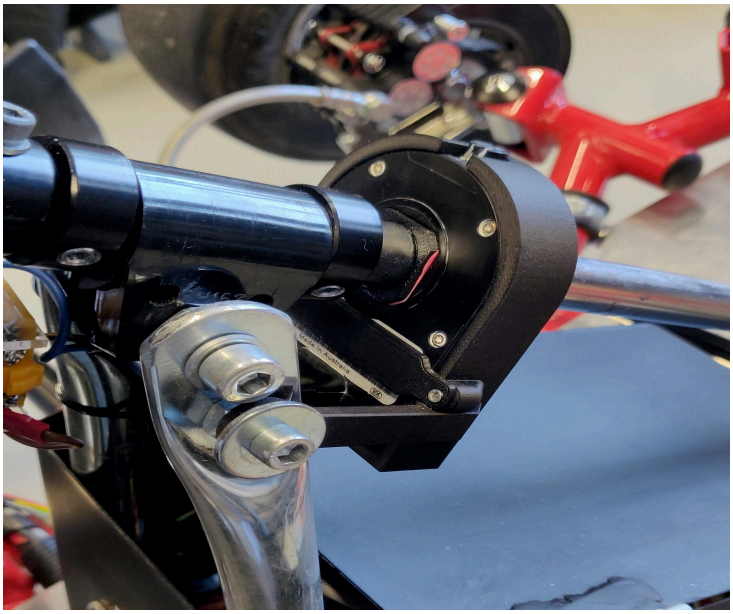

Source: Author (2020).

The message for the steering wheel sensor is detailed at Table 9. Each digit from bytes 0 and 1 represents 0.1°, with hex 94 F9 (Intel) being zero and has an offset of +164.6 to calibrate the zero, and a range of $720°$. Steering right is positive and left is negative from the driver angle.

Table 9 – Steering wheel message.

ID	Byte (Intel)			
0C0	0 1 steering angle	2 3 –	4 5 –	6 7 –

Source: Author (2020).

4.3.3 Acceleration Sensor

Likewise, the acceleration sensor model number is 0 265 005 751 and it is also from Bosch. For its installation, it needs to be settled along the middle axis of the kart. The sensor was fixed inside a box below the steering wheel, along with other electronic equipment as shown in Figure 24.

Figure 24 – Acceleration sensor marked in red.

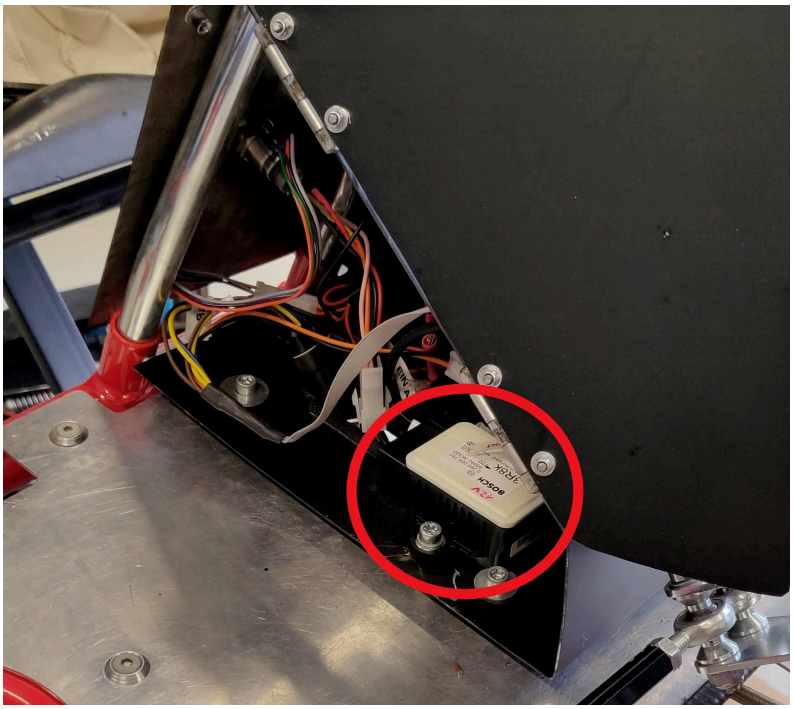

Source: Author (2020).

The acceleration sensor values are not used for the calculus of the controller, but it is really important to keep track of the movement of the vehicle. The sensor message is displayed in Table 10.

Table 10 – Acceleration sensor message.

ID	Byte (Intel)			
130	0 1 omega_z	2 3 –	4 5 acceleration a_y	6 7 –
131	–	–	acceleration a_x	–

Source: Author (2020).

The axis for the sensor are explained in Figure 25, with the sensor being installed so its axis can follow the axis of the vehicle. Factor and offset for the sensor, to be used along with Equation 14, are explained in Table 11.

Figure 25 – Acceleration sensor axis.

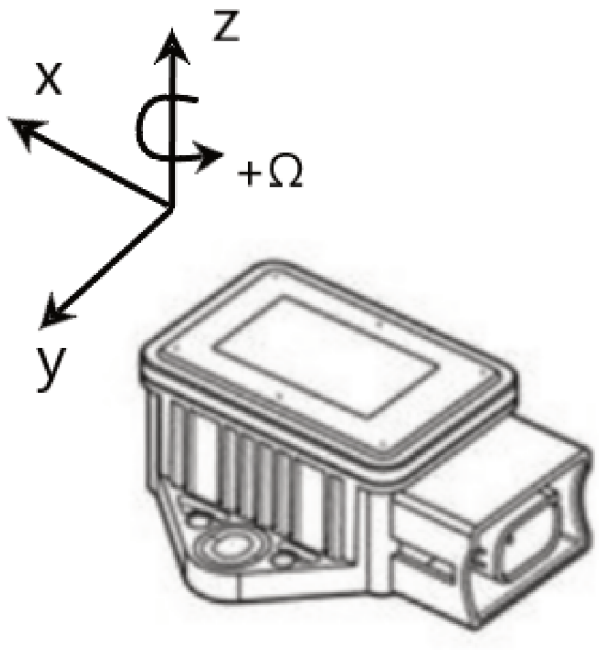

Source: Author (2020).

Table 11 – Factor and offset acceleration sensor.

Variable	Factor	Offset	Format
Acceleration	-0.00125	-32768	m/s^2
Turn Rate	0.005	-32768	$^\circ/s$

Source: Author (2020).

4.3.4 Brake Pressure sensor

The brake pressure sensor was implemented right before the rear brake disc, using new hydraulic cables so the brake fluid could reach the sensor. The model of the sensor is ZS-V2 from Zila Elektronik, and it has a range of 0 to 100 bar, with 0V being 0 bar and 10V is 100 bar. This sensor message is a part of the analog box with ID 250 as already explained at section 4.3.1. The maximum value obtained when braking was about 30 bar. Regarding Equation 14, the values can be found in Table 12.

Table 12 – Factor and offset brake pressure sensor.

Factor	Offset	Format
0.003125	0	bar

Source: Author (2020).

Indeed, the brake pressure sensor was installed near the left rear wheel and attached to the structure of the Kart. An extension to the hydraulic system was built, so the hydraulic fluid could reach the sensor. Figure 26 show where the sensor is installed, near to the cable box at the rear of the Kart.

Figure 26 – Brake pressure sensor installed.

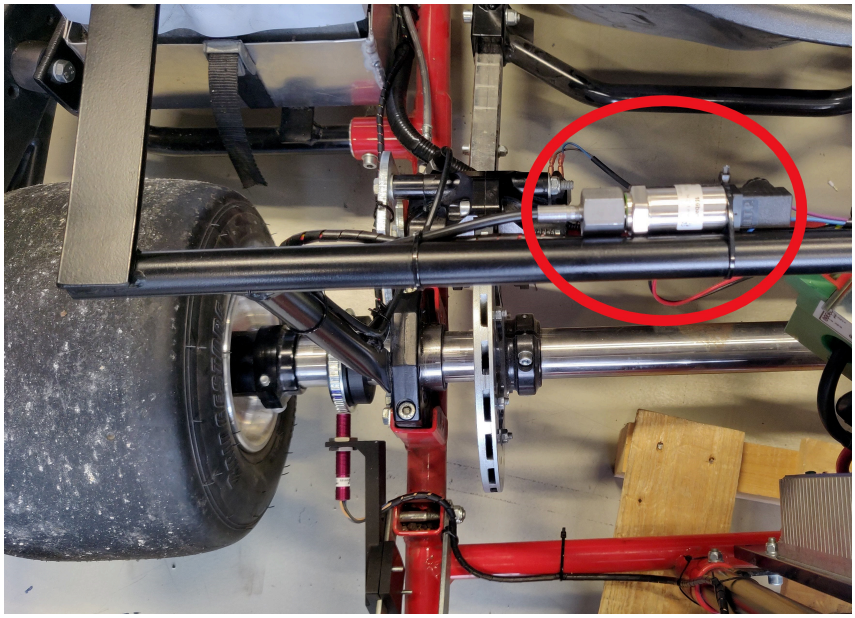

Source: Author (2020).

4.3.5 Motor Voltage/Current and Gas Pedal

Regarding motor voltage, two cables were installed on the DC motor to obtain its voltage. The current coming out of the motor was to high, for this reason a small box with a resistor was installed after the motor, so the size of cables could be reduced, as shown in Figure 27.

Figure 27 – Circuit board to reduce current on cables.

Source: Author (2020).

Both cables coming out of the black box goes directly to the right circuit board as presented in Figure 28. Before feeding this signal to the PCAN Analog 2, a voltage divider was inserted to protect the box from the high voltage coming from the motor and also a capacitor to avoid abrupt variations. At full throttle, it reaches about 48V. So, the voltage divider had two resistors of 5.6kΩ and 1kΩ, generating an output voltage of about 7.27V for the resistor of 1kΩ, when at full speed, to feed into the Analog 2 box.

Figure 28 – Voltage divider protection.

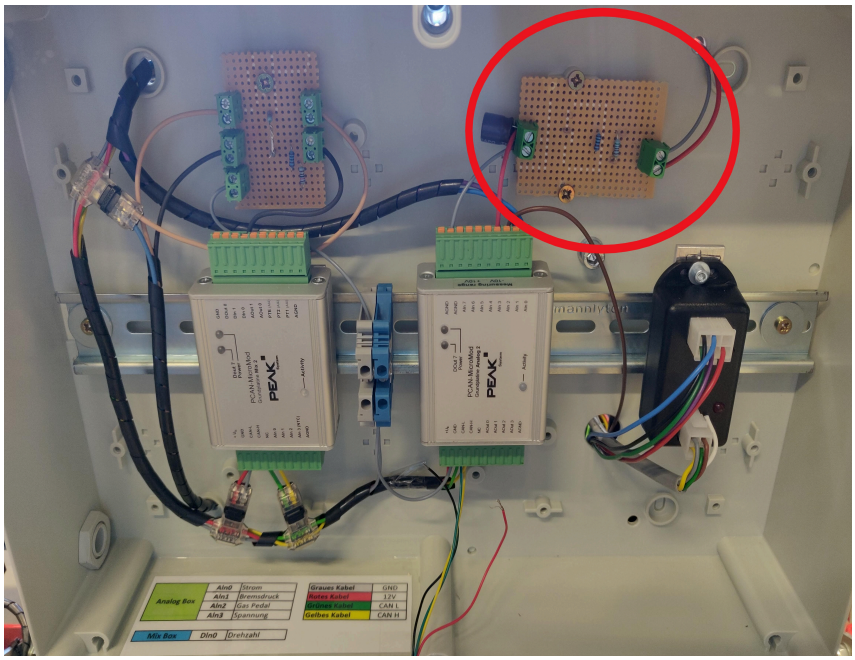

Source: Author (2020).

Furthermore, the current value was obtained through a sensor. The sensor

model is CYHCT-S3 from ChenYang company, with an output of -5V to +5V since it is measuring an AC current. Figure 29 shows how the sensor was installed.

Figure 29 – Current sensor installed.

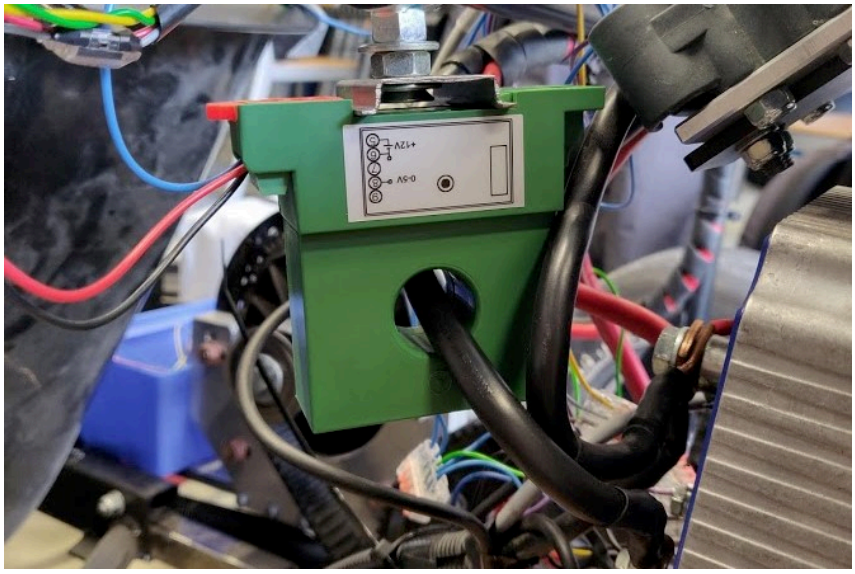

Source: Author (2020).

Additionally, it will be explained in this section the gas pedal too, as its installation was really simple. Since the kart already had a potentiometer installed for the gas pedal, two cables were sufficient to get the output voltage, one for the output signal and the other one as a ground.

In this case, the factor and offset for these sensors are explained in Table 13. For the values disposed below, motor voltage ranges from 0 to 48V, current stays between -150A and 150A, and for the gas pedal it goes from 0 to 5V.

Table 13 – Factor and offset for different sensors.

Variable	Factor	Offset	Format
Voltage	0.00207	0	V
Current	0.00915	0	A
Gas pedal	0.009246	-0.49	V

Source: Author (2020).

4.3.6 Wheel turn rate

Specifically, the turn rate sensor was the only sensor that was installed on the Mix 2 box, due to the output of this sensor being in a frequency format. For its installation, two supports were made in a 3D printer, one to support the sensor

and the other to attach the rear axle and the gear for the measure, as shown in Figure 30.

Figure 30 – Turn rate sensor installed.

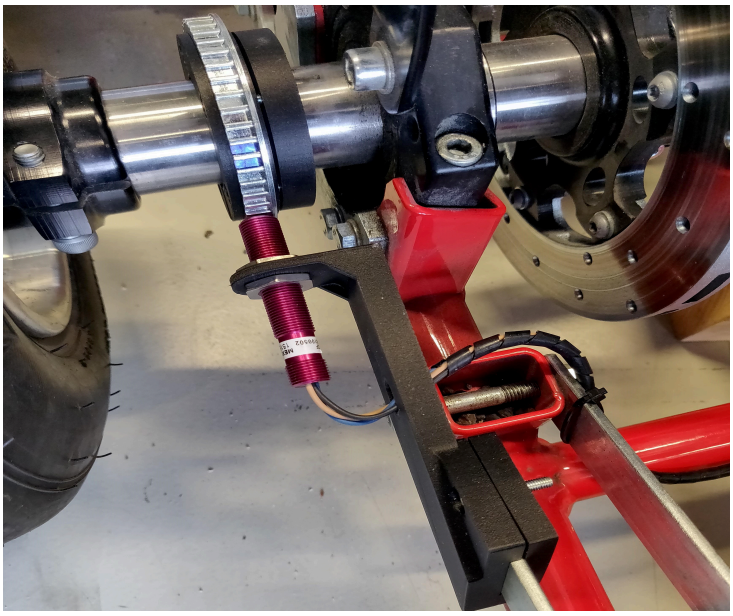

Source: Author (2020).

In this case, this type of sensor needs a gear with a know number of teeth that will spin along with the axle. It will measure if there is a tooth or not, and with that it will display a frequency value, in Hz, as an output. Along with the number of teeth from the gear, it is possible to calculate revolutions/sec, and with that value the velocity in meters/sec. The full process is displayed in Equation 15.

$$V_{\text{wheel}} = 1/\text{n} * 2\pi\text{r} * \text{freq value} \tag{15}$$

n = gear teeth;
r = wheel radius;

Using the wheel radius (r = 0.15 m), gear teeth (n = 48), frequency value from the sensor and doing some simple calculations the result is the velocity of the rear wheel, a very important data for the anti-slip control that was applied in this kart. Replacing previous values in Equation 14, the data for this sensor will be as shown in Table 14.

Table 14 – Factor and offset for turn rate sensor.

Variable	Factor	Offset	Format
Turn Rate	0.019625	0	Hz

Source: Author (2020).

In addition, the digit from this message corresponds to the same value in frequency, for example, if the value is 170 digit, the frequency is 170 Hz.

4.3.7 Kart Velocity

In addition, the velocity sensor was produced according to a bachelor thesis developed by Jonas Schraufstetter along with prof. Harald Göllinger (SCHRAUFSTETTER, 2018). Basically, it consists of two different sensors and an Arduino Nano, just as in Figure 31. Left side of the figure shows the top part of the circuit board with the Arduino, and at the right side both sensors are displayed. All electronic for this sensor was built by the author.

The first one is a high performance optical mouse sensor, type ADNS-3080 from Avago Technologies company. Mouse sensors constantly compare two images from the objective to calculate the relative velocity for the kart. One lens was installed to maximize the distance this sensor can observe, that previously was just 2.4mm.

Figure 31 – Circuit board with Arduino Nano and sensors placed.

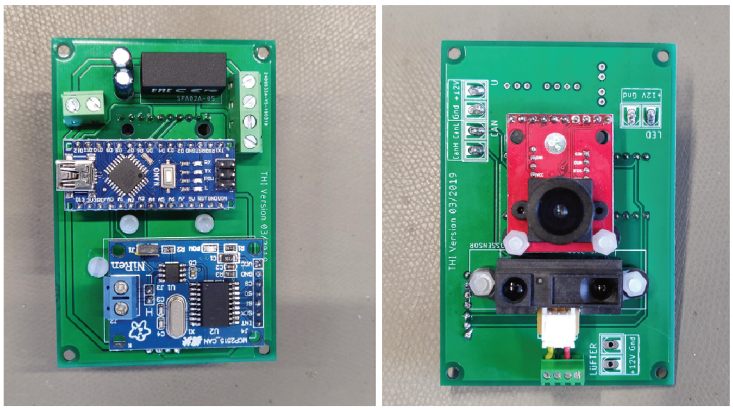

Source: Author (2020).

Along with the optical mouse sensor, a distance measure sensor from Sharp company, type GP2Y0A41SK0F, was placed to check the distance and display it for the Arduino, as well as the values from the mouse sensor. Knowing the value for distance, it helps the mouse sensor to calculate the increments in x and y-axis, when comparing two consecutive images.

The next step after building the circuit board was to print its box. Inside this box will be the circuit board, 6 LEDs to improve images that the sensor will capture, cooling fans and two resistors (SCHRAUFSTETTER, 2018). The box, all of the circuit items and a on/off switch are already positioned and visible in Figure 32.

Figure 32 – Velocity sensor installed.

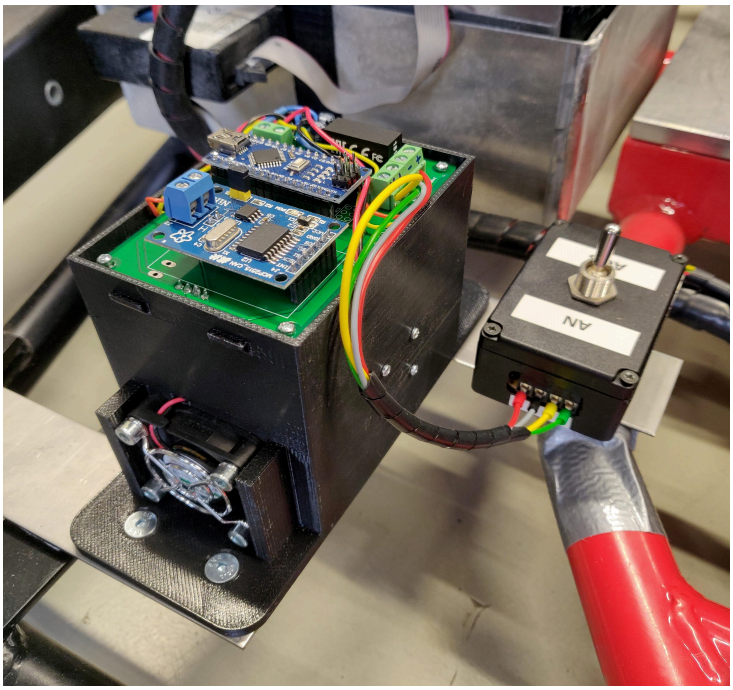

Source: Author (2020).

After all, the code uploaded to the Arduino is responsible to generate the CAN message and send it to the CAN network. The factor of this value is 0.1 since the sensor is measuring at 1600 dpi, therefore, if the value for the velocity bytes are 340, for example, the velocity will be 34 km/h. Observing results from bench tests, the sensor was not measuring with a rate of 400 dpi. With that value of dpi, instead of multiplying by 0.1, to get a velocity value CAN data must be multiplied by 0.025. The ID and which bytes represents the velocity are pointed out in Table 15, as well as factor and offset in Table 16.

Table 15 – Velocity box message.

ID	Byte (Intel)			
	0 1	2 3	4 5	6 7
100	velocity	–	–	–

Source: Author (2020).

Table 16 – Factor and offset for velocity sensor.

Variable	Factor	Offset	Format
Velocity	0.025	0	km/h

Source: Author (2020).

4.4 TRACTION CONTROL CODE AND CONTROLLER CONFIGURATION

After all, in this section, the micro controller used on the tests and the rest of the configuration will be explained, such as the connection from the sensors with the controller and traction control code on Simulink. The micro controller is from Texas Instruments, model TMS320F28379D and is very common. Figure 33 displays the micro controller applied on this thesis and clarifications about the connections that were made.

a) CAN high and CAN low - so the controller can read the messages from all sensors
b) Voltage from the gas pedal - input from the gas pedal for the traction control code
c) I^2C converter ADC4725 - responsible for sending the new voltage, after the traction control is applied, for the electric motor controller
d) Power bank connection - responsible for powering up the micro controller

Figure 33 – Micro controller utilized.

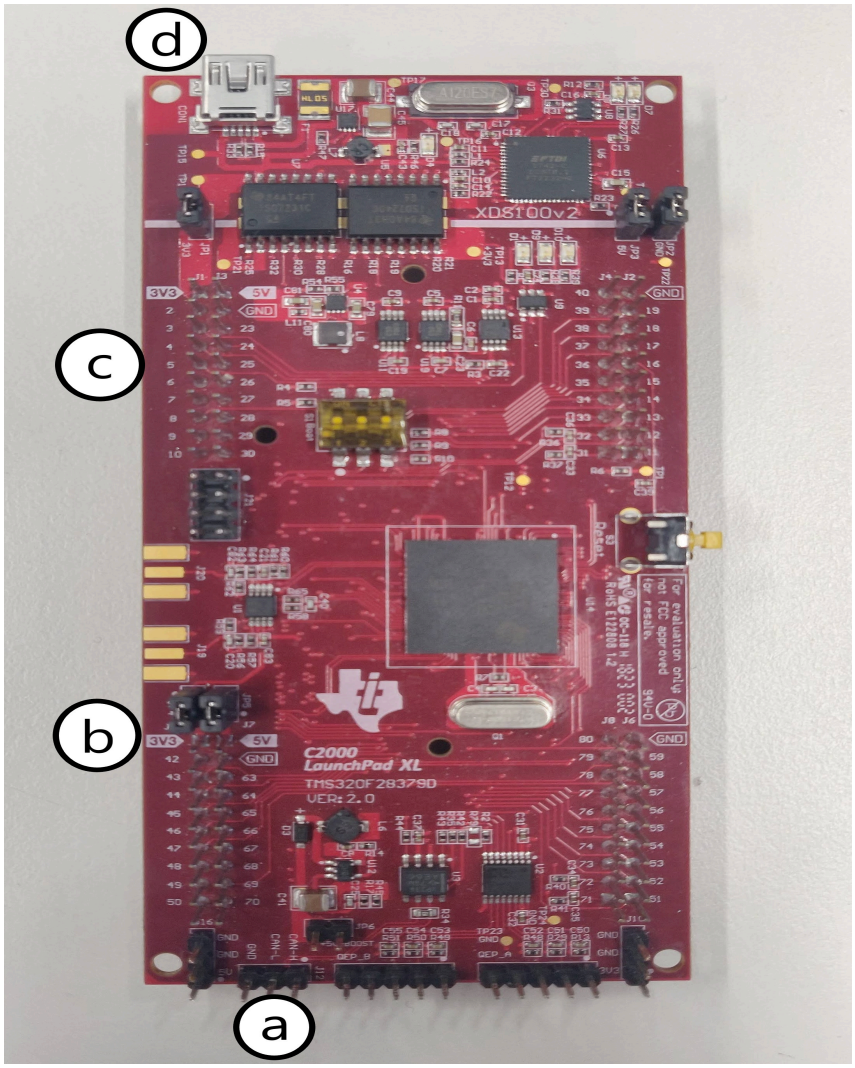

Source: Author (2020).

Moreover, the Simulink code for traction control from Figure 34 was built in the

controller. This step is necessary so the code developed and presented below can run at the micro controller, without the need of Simulink running on a computer. With respect to these tests, a computer was connected to the micro controller in order to power it up, but it could be done with a power bank also.

Figure 34 – Simulink model used for the tests.

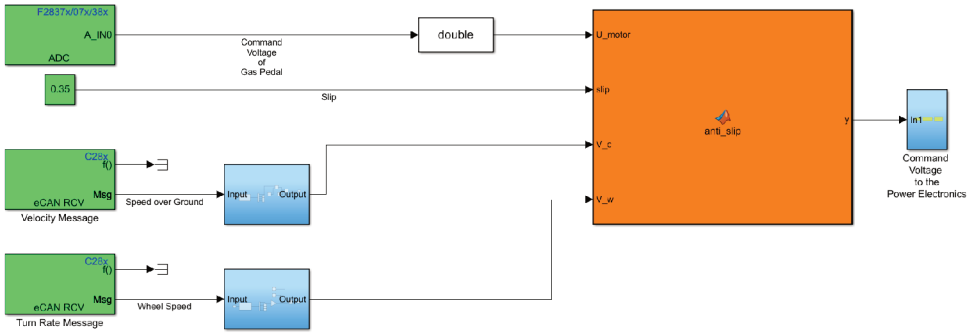

Source: Author (2020).

All green blocks, except from the one with the value 0.35 inside it, are from *Embedded Coder Support Package for Texas Instruments C2000 Processors* package, available to download on any Matlab Simulink. The first block represents the input of the gas pedal from the driver. As explained in Section 4.3.5, the gas pedal produces a voltage signal, ranging from 0 to 5V that is connected to the micro controller. This voltage will be an input for the anti-slip code, and if the wheel spins, the code will decrease it and analyze the new wheel and kart velocity.

The second green block is the slip threshold for the tests. If the slip is bigger than 0.35, the code will act and decrease it to less than 0.35. The third and fourth green blocks are responsible for reading the CAN messages and are from the Texas Instruments package. The block takes the ID from the message as input and will output the hexadecimal value for each byte from that ID.

The blue block, presented after the message blocks, are responsible for unpacking which bytes represent the correct value and also treating it with the factor and offset determined in Section 4.

For the velocity message, bytes 0 and 1 represent the velocity value, the factor is 0.025 and the output will be km/h, so it is also divide by 3.6 in order for it to be m/s. The turn rate message is also presented in bytes 0 and 1, and the treatment for that message is according to Equation 15 and variables given in Section 4.3.6.

The orange block is the traction control code. It takes as input the gas pedal from driver, threshold slip, kart velocity and wheel velocity. The actual slip from the kart will be calculated taking the kart velocity and wheel velocity, accordingly to Equation 1. Having said that this thesis will not cover traction control for braking examples, the code will not act on that case.

Below is a pseudo code, representing the orange block from Figure 34 that contains the code utilized for the anti slip control. As demonstrated above, the code will receive the voltage from the motor as U_motor, the slip threshold, wheel velocity and kart velocity.

Algorithm 1: Anti slip control pseudo code

```
i = 1;
actual_slip = (V_w - V_c)/V_w;
if actual_slip > 0.35 then
    while actual_slip > 0.35 do
        actual_slip = actual_slip * (exp(-(0.18/i)));
        U_motor = U_motor * (exp(-(0.18/i)));
        i = i + 1;
    end
    y = U_motor;
else
    y = U_motor;
end
```

Source: Author (2021).

Analyzing the pseudo code, if the actual slip is bigger than the threshold slip determined before, the code will act on the input gas pedal voltage, reducing it while the slip stays bigger than 0.35. In order to have a stop criteria when reducing the voltage, this code will reduce the slip at the same rate as the voltage from the motor, and after the slip is smaller than the threshold the output y will be U_motor reduced.

Instead of discounting at each run a constant voltage value, Equation 16 is utilized because it will smooth the decay. The furthest the $actual_slip$ is from the threshold, bigger will be the reduce step. As variable i increases at each run of the While loop, the reduce step will be smaller, producing an exponential aspect, rather than a ladder one, if a constant value was reduced at each step.

$$U_{motor} = U_{motor} * \exp\left(-0.18/i\right) \tag{16}$$

In conclusion, if the wheels are not locked and the actual slip is bigger than the threshold, the voltage that is sent to the electric motor will decrease with each step (i) and as a stop criteria, the $actual\_slip$ will also be reduced. The value of 0.18 inside the exponential was acquired through trial and error, testing different values and analyzing the converge of the voltage value.

As explained in Section 2.2.2, rather than a threshold controller, a PID controller could be implemented or even a Sliding mode controller. In this thesis, the threshold

control was chosen due to its simplicity. Despite being simple and easy to implement, it requires many experimental tests to get reasonable thresholds for different road conditions. In this case, a threshold of 0.35 and the factor of 0.18 on the step reduce equation produces a good control, considering the friction coefficient of the tests, variable that is not possible to measure in this thesis.

Furthermore, the PID controller method does not need a specific mathematical model, however it depends on many different control parameters to fully adjust the controller. In a road with special driving conditions, from a high friction coefficient to a low one, the conventional PID controller would produce large control errors, since this slip control problem has a high non-linearity as already discussed.

Sliding mode and fuzzy controllers were not considered due to its complexity to setup it up correctly, with many different tests needed to find the proper control rules, adjustments and still not considering equipment and mathematical models required.

The last block presented in Figure 34 is in control of sending the output voltage value to the electric motor, through the I^2C converter, using a I2C Transmit block, also from Texas Instruments package.

5 RESULTS

In this chapter, all results both from the Simulink model and tests executed are presented and analyzed. Also, before displaying all results, tools and procedures to check if sensors are working properly are discussed.

Firstly, in order to check if the measurement system is receiving and transmitting all messages, and if it is possible to collect data from different sensors, a software named PCAN-Explorer 6 from PEAK-System company was used. With this software it is possible to check if all sensors are working regularly and if the factor and offset are converting regularly from hexadecimal to physical value. Before using PCAN-Explorer 6, it is necessary to create symbols for each sensor that will represent the structure of each message, with inputs like the ID, the position of each value within the message and the factor/offset. The software used for this step is PCAN Symbol Editor 6 and in Figure 35 it is possible to see one example of layout for message ID 250.

Figure 35 – Message ID 250 layout using PCAN Symbol 6.

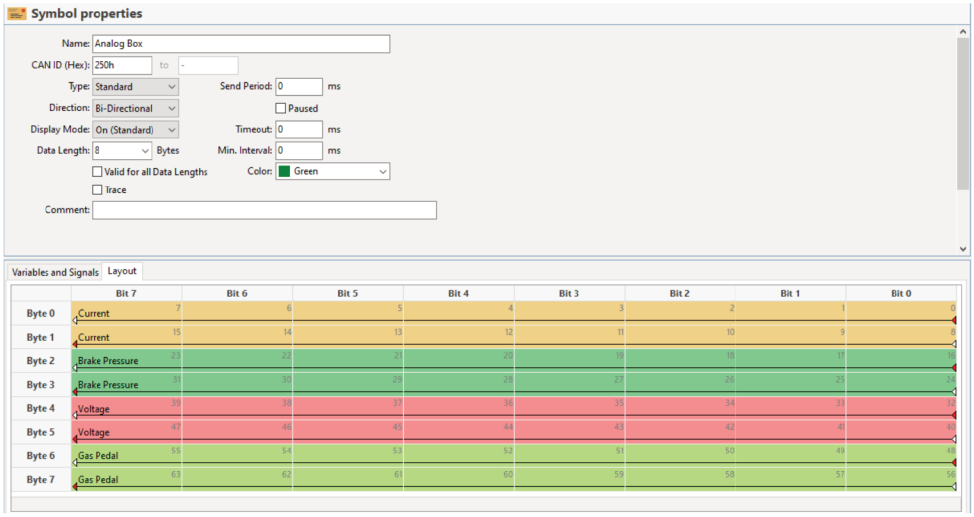

Source: Author (2020).

Afterward, with all symbols created, factors and offsets all set, this file was imported into PCAN-Explorer 6 and Figure 36 shows the layout created to visualize the data and present this research at the AWARE-Center opening ceremony realized 10 of February of 2020, in Ingolstadt - Germany. Through this layout it was possible to check data from some sensors, like steering wheel, brake pressure, kart velocity and that it is possible to acquire data with the measurement system implemented.

Figure 36 – Layout created to visualize data from all sensors.

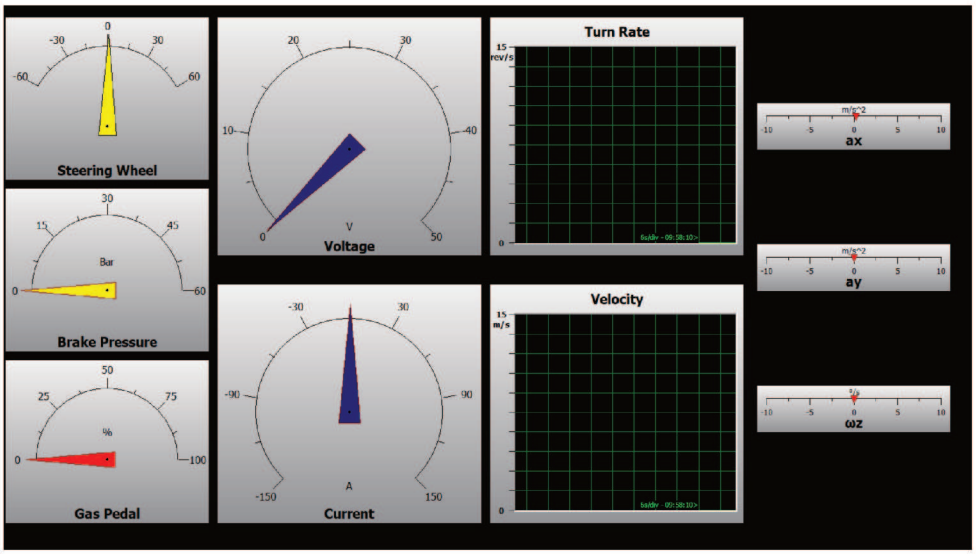

Source: Author (2020).

5.1 SIMULATION RESULTS

In this section, the results from the Simulink model will be presented and validated. Considering the explanation displayed in Section 4.2, the model was built considering physical equations for the electric motor and motion for a steady signal of 5V. Figure 37 given below shows data for kart and wheel velocity, slip and gas pedal with no traction control code.

Figure 37 – Values for Simulink model without TCS.

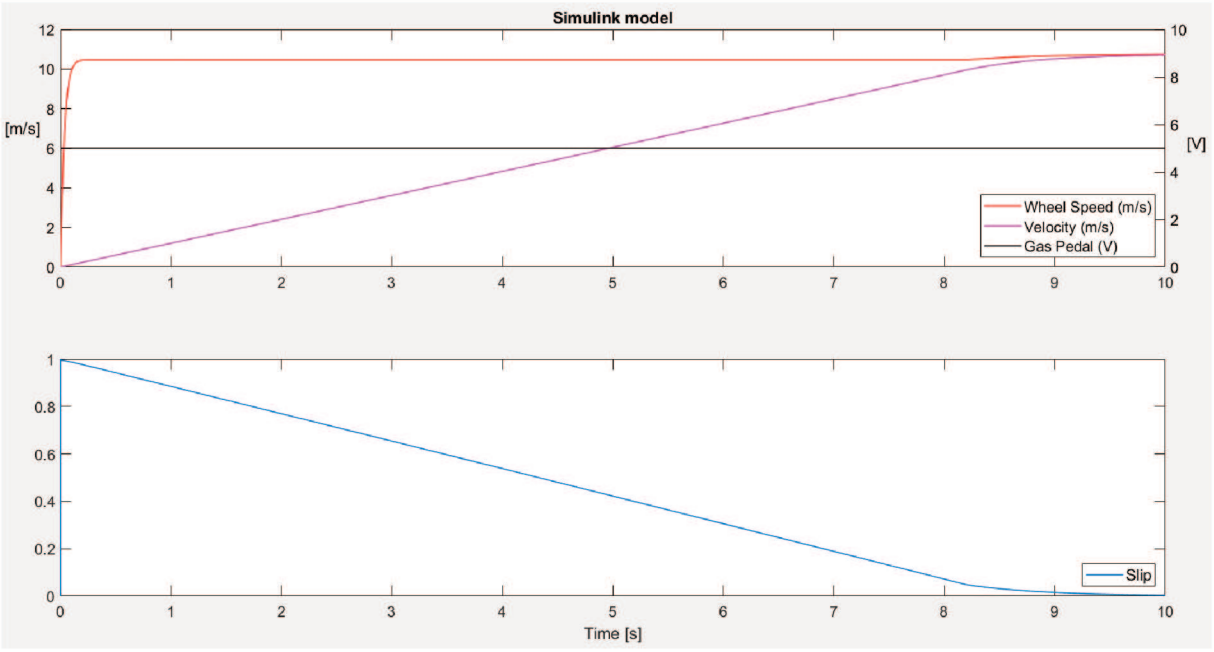

Source: Author (2020).

Throughout Figure 37, it is possible to see that the gas pedal is constant at 5V during the test and the difference between velocities is really high, representing a slipping condition during the whole simulation. Due to a characteristic of electric motors, almost all torque generated from the voltage input is delivered to the wheels, increasing the wheel velocity to its maximum right at the beginning of the simulation. As the model does not consider if the kart is slipping and no traction control code is applied, the difference between both velocities will maintain at a high value during the simulation.

The kart will slowly gain velocity as the torque is delivered and start to overcome all inertia moment and the friction coefficient, with just a small portion being transferred to the track. Close to the end of the simulation, the kart achieves the same velocity as the wheel and maintain that value. At the beginning, slip is close to 1 because linear velocity is really low. When both velocities are equal, slip is zero as there is no difference between both velocities.

Furthermore, the linear velocity of the kart has a small increase mostly because of the friction coefficient (μ) used in this simulation. In this case, for each slip value, there is a coefficient value, ranging from 0 to a maximum of 0.25, simulating a snow path. It is Above all, the model worked as expected.

Knowing that the model is performing as expected, the traction control code explained earlier is implemented on the Simulink as Figure 38 shows. The only difference from the model below to the one discussed in Section 4.2 is the presence of the traction control code, the same one used during tests and explained in Section 4.4.

Figure 38 – Simulink model with traction control code.

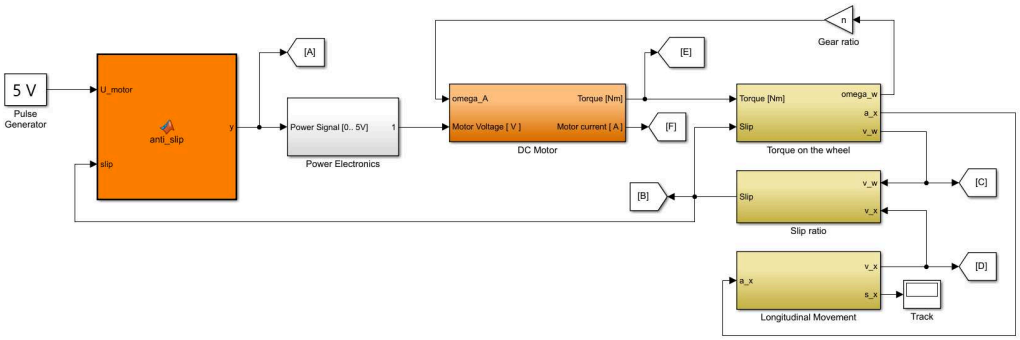

Source: Author (2020).

With this in mind, Figure 39 presents the results for the Simulink model of the kart with a traction control code. As elucidated before, that code will act on the gas pedal voltage sent to the electric motor and will reduce the velocity difference between wheel and kart.

Figure 39 – Values for Simulink model with control.

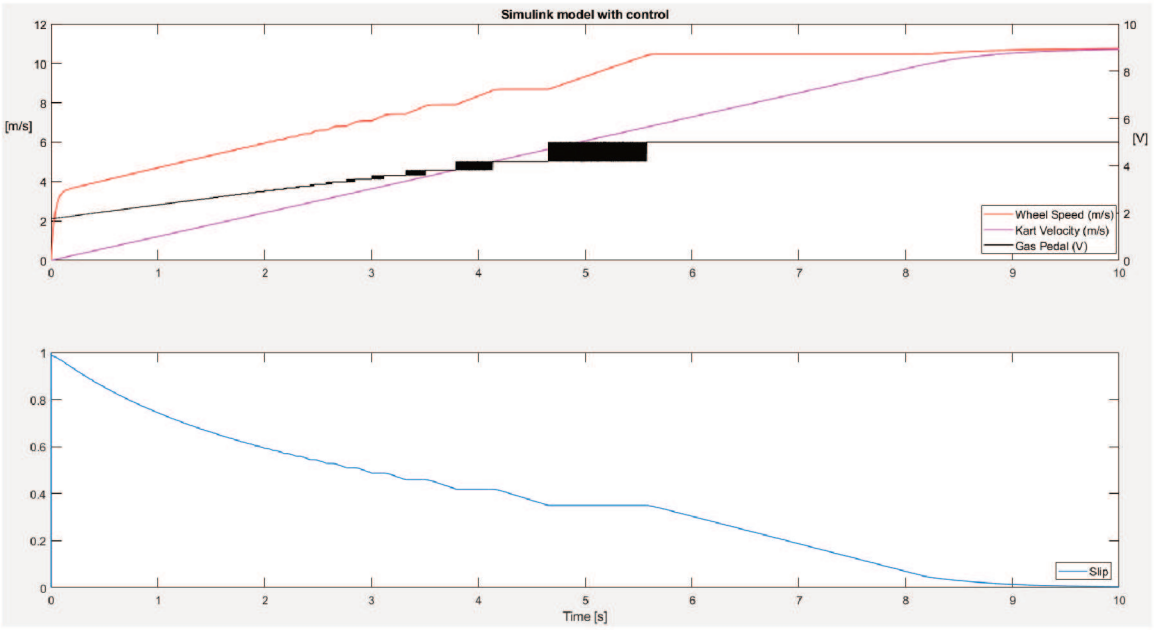

Source: Author (2020).

Analyzing Figure 39, the slip decay rate is really low, taking about 4 seconds for the slip to go from 1 to about 0.45. The main cause for this poor performance is due to the friction coefficient used in this run of the model. The range of friction coefficient used in Figure 39 was from 0.2 to 0.25, simulating a snow path, however for this situation the performance of the controller is poor. After increasing the friction coefficient in about 3 times, the results are presented below in Figure 40

Figure 40 – Values for Simulink model with control with higher friction coefficient.

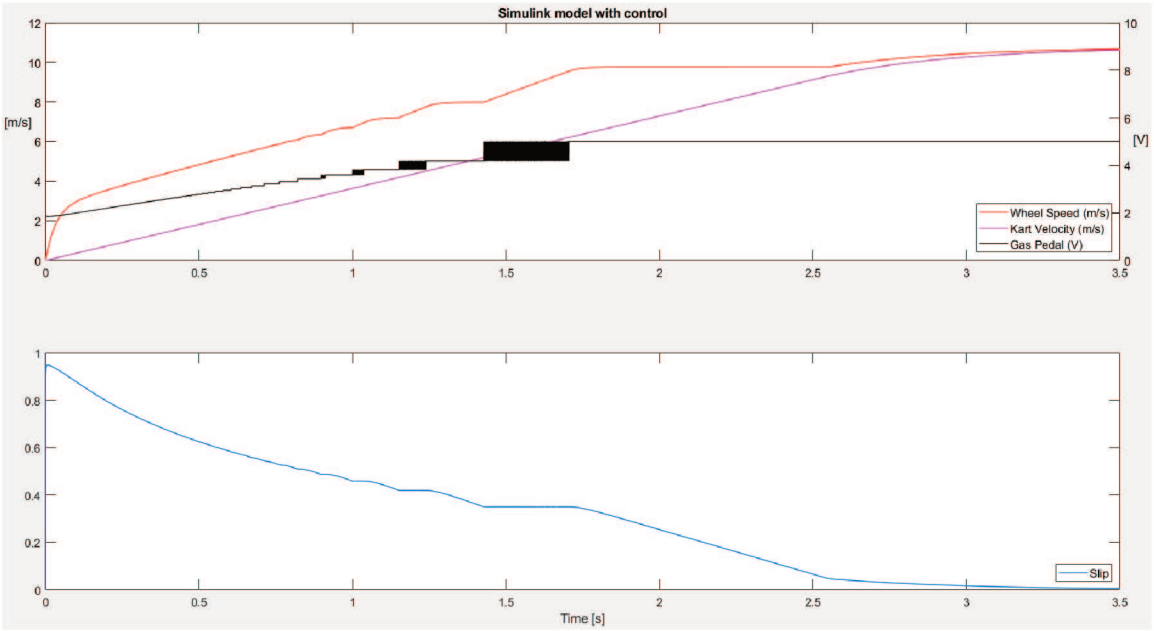

Source: Author (2020).

With this new value of coefficient, the time to achieve maximum velocity went from about 9 seconds to 2.7 seconds, with just 1.4 seconds to go from slip equal 1 to 0.35. Also, as the adhesion is higher for this run, wheel velocity has a smaller rate when comparing to Figure 39 because more torque is transferred to the ground.

Analyzing the code, at the start of the simulation it will prevent the spike at the wheel velocity, trying to achieve the threshold slip of 0.35 discussed early. Since the slip is really far from the threshold and the further it is, more accurate the step will be, thanks to the exponential function used, the slip is tending to 0.35.

At the time that the slip is closer to the threshold value, with just one step of the exponential function the slip will be less than 0.35. The black region near 5 seconds on the gas pedal shows that. With one step, the output voltage will be 4.61 and the slip will be smaller than 0.35. When the motor receives this voltage, the wheel will have a lower speed, consequently reducing the skid also. Coupled with the wheel not skidding anymore, the kart will be able to accelerate more, trying to use most of the torque it receives and when it uses all 5 V, the slip will increase again triggering the code once more to reduce the voltage.

In other words, the region where the gas pedal voltage ranges between 4.61 and 5 V in a short period is where the code works. It keeps a desired slip while trying to maximize the torque transferred to the track. The behaviour is similar to what is observed on ABS brakes, locking and unlocking wheels in a short time to keep traction and preventing skidding.

5.2 TEST RESULTS

In the same way, real tests were performed with the code already explained in Figure 34 previously and using the same test setup explained in Section 3.

While the friction coefficient (μ) value for the simulation ranged between 0.7 to 0.75, it is not possible to precisely measure it for this test, since it depends a lot on the relation between tyre and carpet in this case.

Different tries were executed with this setup, gathering as much data as possible. The first trial was produced without the anti-slip code, in order to evaluate if the kart would skid as predicted. All tests were executed with a computer connected to the micro controller, the kart starting at the beginning of the carpet, just as Figure 12 shows, and the throttle pedal was fully pressed for the whole test. Both rear wheels drifted due to the high torque, hence leading the kart to loose its rear end and rotate around axle Z, just as Figure 41 presents.

Figure 41 – Kart after rotating without anti slip control.

Source: Author (2021).

Following the tests without control, where the Kart lost its rear end, next tests were performed with the controller applied and the results were saved on the computer. The first test realized did not produced the results expected. Figure 42 below shows the motor voltage, velocity for the kart and wheel and slip.

Figure 42 – Graphs from the first test of the controller.

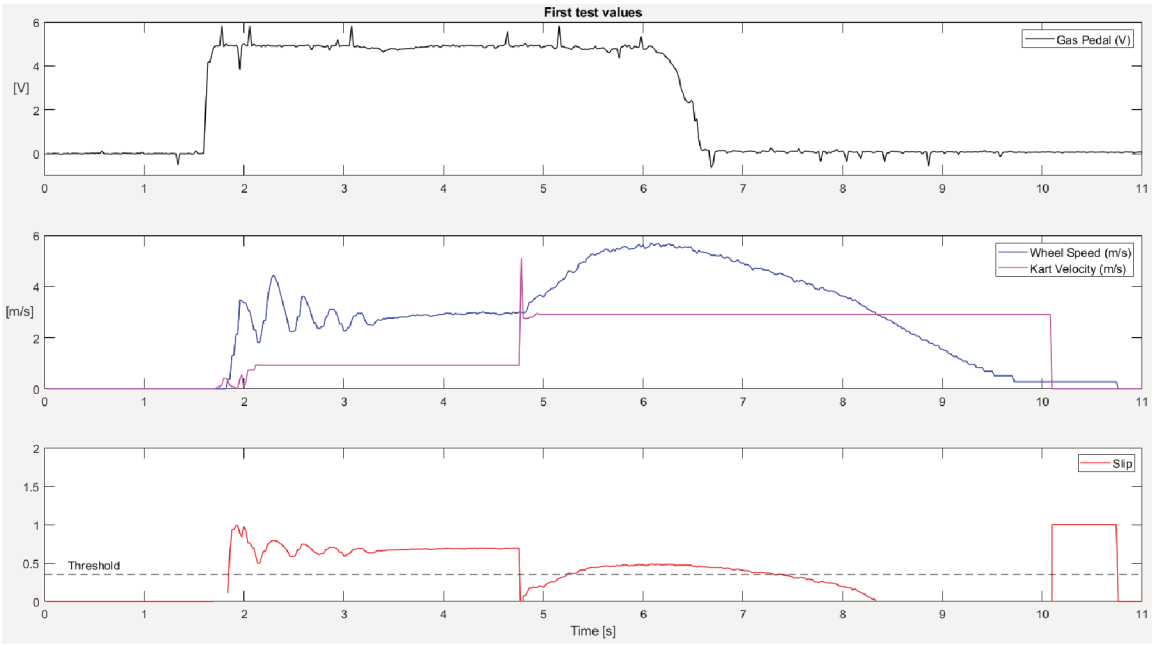

Source: Author (2021).

Analyzing Figure 42, the kart velocity presents an unexpected behavior, not increasing along with wheel speed and is constant during most of the test. On the other hand, wheel speed has a nice behavior, oscillating at the beginning trying to reach the threshold desired, and after it enters a part of the carpet that has a higher friction coefficient, the wheel speed increases.

With the aim of understanding this problem with velocity variable, the sensor was bench tested again to investigate the values from first test, and in conclusion, the problem was with the acquisition rate from the mouse sensor. Instead of collecting data with 1600 dpi, it was using 400 dpi, resulting in an output velocity of one quarter of the expected. Since the velocity sensor measures the difference of two images in a sequence, it is susceptible to vibration from the road and even the layout of the surface below. Taking that into account, the carpet was switched to bring more difference in images from the x-axis, like a layout using strips with different colors.

Further tests were performed with the traction control applied to the micro controller and after correcting the velocity sensor, the values are displayed in Figure 43.

Figure 43 – Test values after corrections in the velocity sensor.

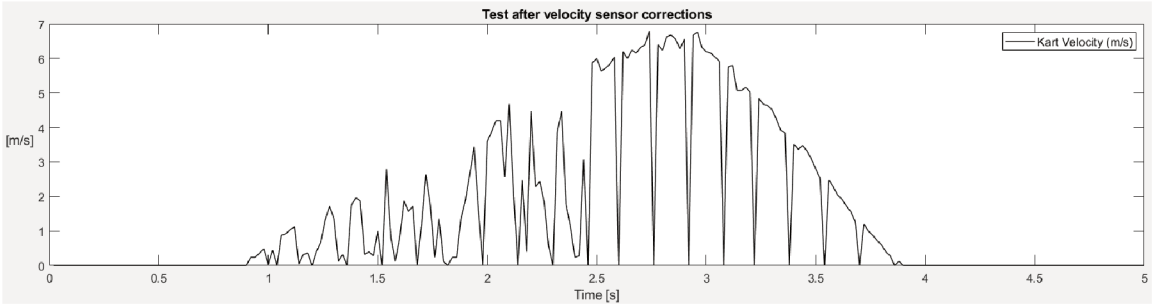

Source: Author (2021).

Even though the acquisition rate of the velocity sensor was adjusted and a new carpet was used to perform this test, kart velocity is very unstable, going to zero several times during the test. The curve of velocity is a lot better than the previous test, however it is not good for the controller to analyze and take the best decision based upon that data. Taking that into account, it was used the integral of the acceleration sensor from Bosch, a much more reliable sensor than the mouse sensor, representing velocity of the kart.

Consequently, adjustments were made into the controller, in order to use the integration of the acceleration as kart velocity and the results for this final test are displayed in Figure 44.

Figure 44 – Final test results.

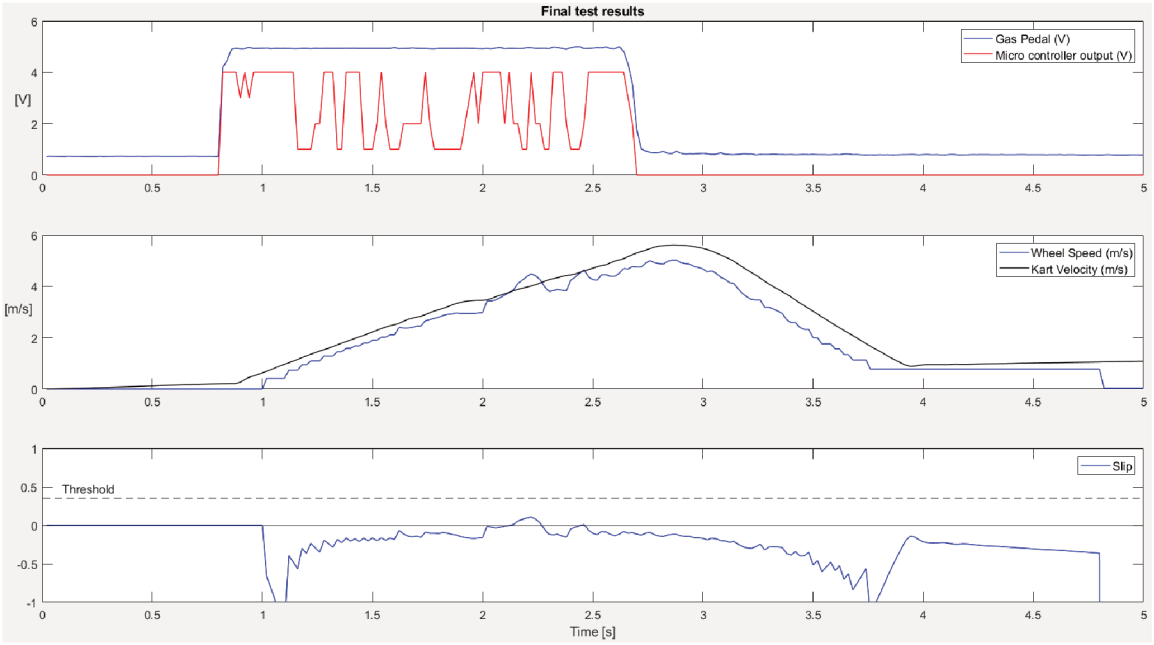

Source: Author (2021).

First graph presents the voltage generated from the accelerator. The blue line shows that throughout the test, the gas pedal stays 5 V, representing full throttle. In red is the output from the micro controller, after the code processing.

Moreover, second graph contains wheel velocity and kart velocity, necessary for slip calculation. Along with, the third graph exhibits the slip, as well as the threshold value. Velocity values are producing a negative value of slip, meaning the kart velocity is bigger than the wheel speed, just like a brake slip. This behavior was not expected and analyzing carefully all this data, some points were noticed. At the start of the test, where the kart is not being accelerated and at the end, when the kart is fully stopped, kart velocity is not zero as it should be. Evaluating the acceleration sensor, it was observed that it had a small angle over the horizontal plane, close to $1.5°$. Taking that into consider and converting that angle into m/s^2, a small offset of -0.22 was reduced from the velocity curve.

Also, investigating the wheel speed data, the sensor displays a mean value every 0.2 seconds, counting the number of teeth in that period and displaying a mean value of velocity. Considering that, this sensor is always 0.1 seconds behind the kart velocity for example, and to compare both velocities at the exact same time, an offset of 0.1 seconds was also reduced from the wheel speed curve, moving it to the left of the graph.

Given the above data treatment, Figure 45 represents the final graph with all treatment explained before, post processing the data acquired from the previous test.

Figure 45 – Final test results after corrections.

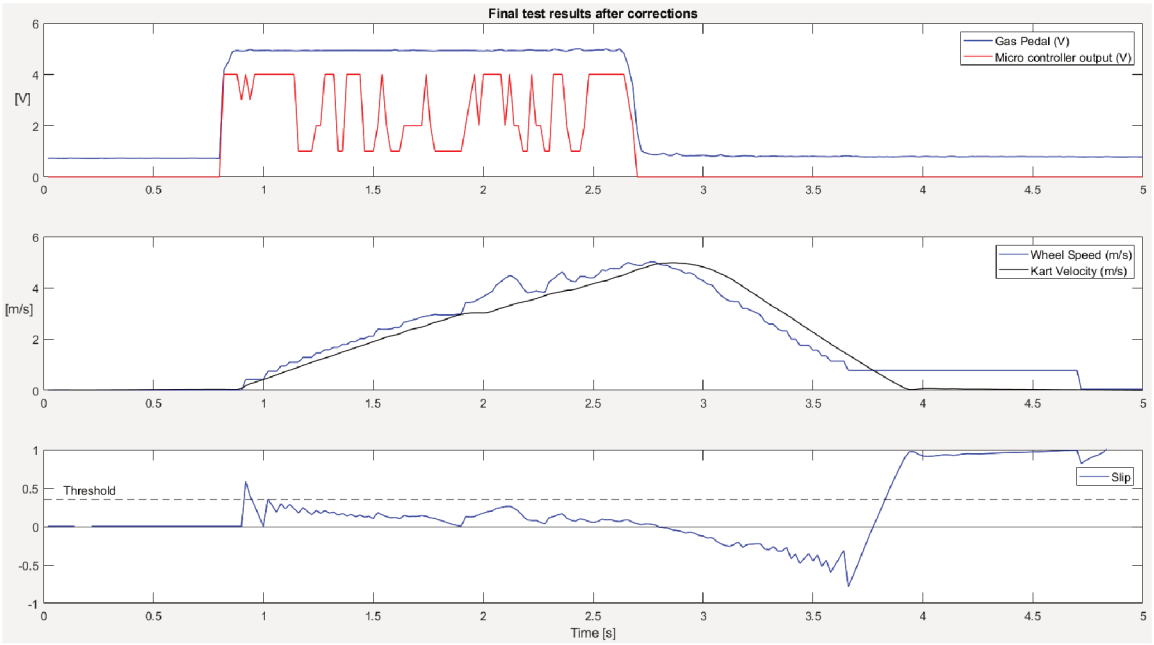

Source: Author (2021).

At the start of the test, the wheel velocity increases as the gas pedal is fully pressed, however, as soon as the code realizes the difference is getting higher, it reduces one step from the voltage twice near 1 second, and after that it keeps sending 4 volts, according to the offset used on gas pedal. With this higher voltage level, the wheel velocity continue to raise and the kart remain with a low velocity due to the slip. From 1 second close to 2.5 seconds, the code is increasing and decreasing the motor voltage, trying to maximize the torque that can be transferred to the wheel without slipping above the threshold of 0.35.

That performance occurs again three times between 2 and 2.5s, with the code reducing the voltage in steps to keep the slip in the desired range, consequently reducing the difference between velocities and causing the code to increase the voltage.

Just before 3 seconds, the kart is not accelerating anymore and brake is pressed, explaining why wheel speed goes below kart velocity and slip is negative. After 3.5 seconds, the wheel speed sensor had a breakdown sending a constant value for about 1 second, even though the test was already finished, and with that the slip went to really high positive values.

Correspondingly, the slip presents a similar behaviour as the voltage when evaluating it. Just after the start of the test, the wheel and kart velocity are really far, as wheel velocity has a small spike, resulting in a slip higher than the threshold determined. This higher slip results in a reduce of the voltage value, decreasing wheel velocity and consequently slip. With a small slip, the code increases voltage of the motor as it can transfer more torque, and when slip gets close to 0.35, it lowers the voltage again with

this cycle happening during the whole test.

All things considered, Figure 46 presents a graph comparing values from test and Simulink model. Despite the fact that the duration of the test and model is not the same, with about 5 seconds and 3.5 seconds respectively, the model graph was extended until 5 seconds, so both curves can have its design compared.

Figure 46 – Overlapped graphs comparing velocities from model and tests.

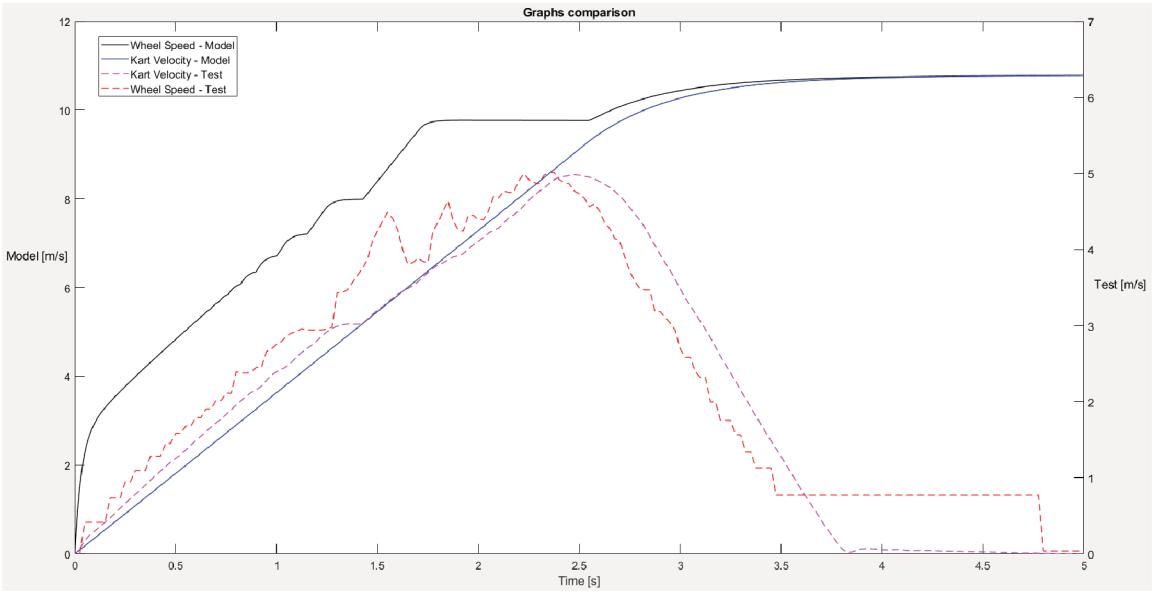

Source: Author (2021).

Both kart and wheel velocity have a similar curve pattern, even though the test has velocities with values scaled down when comparing with the model, since the test stands with a maximum of 5 m/s and model values with 10 m/s. This discrepancy can be explained by the friction coefficient used on the simulation, ranging from 0.7 to 0.75, and the one established on the test that could not be measured and was not the objective of this thesis. With different friction coefficients used on each case, different traction forces were transmitted to the path, resulting on divergent values, but with a similar behavior as shown in Figure 46.

6 CONCLUSION

Considering all of the presented throughout this thesis, a traction control system was developed, implemented on an electric kart and validated with tests. The acquisition system built receives and transmits messages in a proper way, and is robust meaning different sensors can be installed in this system, inspecting other variables.

The Simulink model provides a powerful tool to simulate the kart in different environments taking into account variables such as friction coefficient, kart measurements and motor specs. It works with or without an anti slip control code, making it good for different purposes, not just in an anti slip case.

Kart tests were performed in order to validate the Simulink model with real values. After several tests with a traction control code, the kart was able to run and control voltage from the motor to surpass a slippery path, considering this case, where it is used a slippery carpet with water, determining the threshold and working fine. Since this thesis used the threshold control method, that requires several tests for different road conditions, other improvements could be to use other controllers, such as fuzzy controller, sliding mode control or even both as shown in recent studies. With a validated model, they can be tested without the need to setup a real test, being able to find proper control rules designing a robust controller.

Finally, since the main objective of this thesis was to develop and validate an anti slip control code also checking its feasibility, this work provides the confirmation for that question. Using simple equipment and a simple control method, the kart performed well during bad road conditions. Other path conditions, sensors and control methods could be implemented in order to improve it and also keeping it simple.

Considering possible future works, there are a few points that can be explored and improved. The measurement system can be improved with better developed sensors, focusing on a sensor to measure linear velocity, as this thesis presented can be a difficult point to calibrate and obtain correct values. Analyzing the controller, other controller methods can be developed and tested using the tool created in this thesis. Sliding mode control is one that is really robust, widely studied nowadays and can have its impact in the kart analyzed using the Simulink model.

REFERENCES

AGA, M.; OKADA, A. Analysis of vehicle stability control (vsc)'s effectiveness from accident data. In: NATIONAL HIGHWAY TRAFFIC SAFETY ADMINISTRATION. **Proceedings: International Technical Conference on the Enhanced Safety of Vehicles**. [S.l.], 2003. v. 2003, p. 7–p.

ALY, A. A. et al. An antilock-braking systems (abs) control: A technical review. **Intelligent Control and Automation**, Scientific Research Publishing, v. 2, n. 03, p. 186, 2011.

ASMO GMBH. **Design and Realisation of Battery Powered Drivetrains**. Beinwil, 2020. Disponível em: http://www.asmokarts.com/index.cfm?pageID=24. Acesso em: 04 dez. 2020.

AUSTIN, L.; MORREY, D. Recent advances in antilock braking systems and traction control systems. **Proceedings of the Institution of Mechanical Engineers, Part D: Journal of Automobile Engineering**, Sage Publications Sage UK: London, England, v. 214, n. 6, p. 625–638, 2000.

BOSCH, R. **Manual de tecnologia automotiva**. São Paulo: Editora Blucher, 2005.

CORRIGAN, S. Introduction to the controller area network (can). **Application Report SLOA101**, p. 1–17, 2002.

FARMER, C. M. New evidence concerning fatal crashes of passenger vehicles before and after adding antilock braking systems. **Accident Analysis & Prevention**, Elsevier, v. 33, n. 3, p. 361–369, 2001.

GENTA, G.; MORELLO, L. **The automotive chassis**. Berlin: Springer, 2009. v. 1.

GILLESPIE, T. D. **Fundamentals of vehicle dynamics**. Warrendale: SAE International, 1992. v. 400.

HART, P. Abs braking requirements. **Hartwood Consulting Pty Ltd, Victoria**, 2003.

ISO. 11898: Road vehicles| interchange of digital information| controller area network (can) for high-speed communication. **International Standards Organization, Switzerland**, 1993.

KANG, M. et al. Coordinated vehicle traction control based on engine torque and brake pressure under complicated road conditions. **Vehicle System Dynamics**, Taylor & Francis, v. 50, n. 9, p. 1473–1494, 2012.

KAWABE, T. et al. A sliding mode controller for wheel slip ratio control system. **Vehicle system dynamics**, Taylor & Francis, v. 27, n. 5-6, p. 393–408, 1997.

LI, H.-Z. et al. Pid plus fuzzy logic method for torque control in traction control system. **International Journal of Automotive Technology**, Springer, v. 13, n. 3, p. 441–450, 2012.

LIE, A. et al. The effectiveness of esp (electronic stability program) in reducing real life accidents. **Traffic Injury Prevention**, Taylor & Francis, v. 5, n. 1, p. 37–41, 2004.

LIU, G.; JIN, L. A study of coordinated vehicle traction control system based on optimal slip ratio algorithm. **Mathematical Problems in Engineering**, Hindawi, v. 2016, 2016.

LYCKEGAARD, A.; HELS, T.; BERNHOFT, I. M. Effectiveness of electronic stability control on single-vehicle accidents. **Traffic injury prevention**, Taylor & Francis, v. 16, n. 4, p. 380–386, 2015.

PARK, J. H.; KIM, C. Y. Wheel slip control in traction control system for vehicle stability. **Vehicle system dynamics**, Taylor & Francis, v. 31, n. 4, p. 263–278, 1999.

SAVARESI, S. M.; TANELLI, M. **Active braking control systems design for vehicles**. Berlin: Springer Science & Business Media, 2010.

SCHERF, H. **Modellbildung und Simulation dynamischer Systeme: eine Sammlung von Simulink-Beispielen**. Karlsruhe: Oldenbourg Verlag, 2011.

SCHRAUFSTETTER, J. **Implementierung eines Sensors zur Geschwindigkeitsmessung eines Elektrokarts unter Verwendung des optischen Flusses**. Tese (Bachelor's Thesis) — Technische Hochschule Ingolstadt, 2018.

TINDELL, K.; HANSSMON, H.; WELLINGS, A. J. Analysing real-time communications: Controller area network (can). In: CITESEER. **RTSS**. San Juan, 1994. p. 259–263.

WELLSTEAD, P.; PETTIT, N. Analysis and redesign of an antilock brake system controller. **IEE Proceedings-Control Theory and Applications**, IET, v. 144, n. 5, p. 413–426, 1997.

WIBEN, R.; ANDERSEN, M.; JENSEN, H. Design of slip-based active braking and traction control system for the electric vehicle qbeak. **Aalborg University**, 2012.

YAMAMOTO, A.; KIMURA, Y. Influence of abs on rollover accidents. In: NATIONAL HIGHWAY TRAFFIC SAFETY ADMINISTRATION. **Proceedings: International Technical Conference on the Enhanced Safety of Vehicles**. [S.l.], 1996. v. 1996, p. 779–786.

APPENDIX A - MATLAB CODE TO INITIALIZE VARIABLES

```
%Variables Initialization
m = 200; % kg
g = 9.81; % m/s^2
r = 0.135; % m - effective wheel radius

%Lynch 200-127
R_A = 0.0225; % armature resistance [Ohm]
L_A = 23e-6; % armature inductance [H]
k_g = 0.15; % torque constant [Nm/A] = [Vs]
J_A = 0.0236; % [kg/m^2]

% Engine efficiency
current = [ 0 10 20 30 40 50 60 70 80 90 100 110 120 130 140 150 200 220 250 270
300];
eff = [ 30 50 66 74 77.5 80 81.5 82 83 83.5 83.7 83.5 83.5 83.5 83 82.5 81 80 78.5 78
76.2];
eff = eff/100; % from percent -> floating numbers

i_A= 0:10:200; % Armature currents [A] and appropriate torques
Torque= k_g * i_A .* interp1(current,eff,i_A);

n = 20 / 5; % Gear ratio

% Moment of inertia rear wheel
% Cylinder 0.5*m*r^2 + 2* Half cylinder 0.5*m*(r_2^2+r_1^2)
J_R = 0.5*5*0.015^2 + 2* 0.5*1.982*(0.135^2+0.06^2); % kg m^2

% mu-slip curve
% Snow path
slip = (0:.05:1.0);
mu = [0 .25 .2495 .2495 .249 .249 .2485 .2485 .248 .248 .2475 .2475 .247 .247 .2465
.2465 .246 .246 .2455 .2455 .245];
```